Applied Energy 376 (2024) 124280

Contents lists available at ScienceDirect

Applied Energy

journal homepage: www.elsevier.com/locate/apenergy

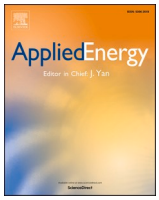

Design and assessment of a concentrating solar thermal system for industrial process heat with a copper slag packed-bed thermal energy storage

Marco A. David-Hernández [a,*], Ignacio Calderon-Vásquez [b], Felipe G. Battisti [c], José M. Cardemil [b], Antonio Cazorla-Marín [a]

[a] Instituto Universitario de Investigación de Ingeniería Energética (IUIIE), Universitat Politècnica de València, Valencia, Spain
[b] Department of Mechanical and Metallurgical Engineering, Pontificia Universidad Católica de Chile, Santiago, Chile
[c] Departamento de Mecánica, Facultad de Ingeniería, Universidad Tecnológica Metropolitana, Santiago, Chile

HIGHLIGHTS

- Integration of a SHIP system with copper slag packed-bed TES
- Dynamic simulation and analysis of the system's main variables
- System performance assessment and control improvement
- Techno-economic analysis of the entire system and carbon savings
- SHIP system with TES presents a payback of 14 years and annual savings of 30 tCO2

ARTICLE INFO

Keywords:
Thermal energy storage
Packed-bed
Copper slag
Dynamic simulation
Techno-economic assessment
Solar process heat

ABSTRACT

Decarbonising the industrial sector is a key part of climate change mitigation targets, and Solar Heat for Industrial Process (SHIP) is a promising technology to achieve this. However, one of the drawbacks of SHIP systems is that they rely on an intermittent energy source. Therefore, sensible energy storage has emerged as a potential solution. In addition, solid byproducts have been proposed as a low-cost but effective material for thermal energy storage (TES). This work presents a SHIP system model coupled with a copper slag-packed-bed TES (PBTES) model using air as heat transfer fluid. The TES has been implemented to preheat the makeup water of the tank where steam is generated. A system design was carried out using a parametric analysis to find a solar field size and a corresponding TES volume. The resulting system was simulated, and the operating variables were analysed in detail. The results show that it is possible to generate 20% more energy due to the storage system. Additionally, a techno-economic analysis indicates that the SHIP with PBTES system results in a payback period of 14 years and a savings of CO_2 emissions of 30 $t\ CO_2$.

1. Introduction

By 2021, the industrial sector accounted for 30% of global energy consumption, of which 63% came from fuels such as natural gas [1], which is mostly used to supply energy in the form of heat to processes. In addition, heat in the medium temperature range (150 $^{\circ}C$ - 400 $^{\circ}C$) represents an opportunity to reduce the carbon footprint of the industrial sector.

Solar thermal energy is a promising solution for decarbonizing industrial processes. In Ref. [2], the authors discuss solar heating for industrial processes (SHIP) and outline the leading countries that use it on a large scale. SHIP's integration strategies are reviewed in Ref. [3]. It covers integration points, aspects of solar collectors, installed capacity, and thermal energy storage (TES) volume. The authors compared integration locations of SHIP for different sectors to determine the most used

Abbreviations: DNI, Direct Normal Irradiance; IAM, Incident Angle Modifier; ISG, Indirect Steam Generation; KPI, Key Performance Indicator; PBTES, Packed-Bed Thermal Energy Storage; SHIP, Solar Heat for Industrial Process; TES, Thermal Energy Storage.

* Corresponding author.
E-mail address: mdavid@iie.upv.es (M.A. David-Hernández).

https://doi.org/10.1016/j.apenergy.2024.124280
Received 22 April 2024; Received in revised form 20 June 2024; Accepted 16 August 2024
Available online 22 August 2024

Nomenclature

A	Area (m^2)
Cl	Cleanliness factor
C_{min}	Minimum heat capacity rate (W/K)
E	Energy (J)
eff	Effectiveness
h	Specific enthalpy (J/kg)
h_v	Volumetric heat transfer coefficient ($W/(m^3 \cdot K)$)
k	Thermal conductivity ($W/(m \cdot K)$)
$\dot{m}$	Mass flow (kg/s)
N_{mod}	Number of modules
P	Pressure (Pa)
$\dot{Q}$	Heat rate (W)
s	Thickness (m)
T	Temperature (K)
t	Time (s)
U	Overall heat transfer coefficient ($W/(m^2 \cdot K)$)
Z	Utilisation factor

Greek symbols

ε	Void fraction
η_0	Optical efficiency
θ	Angle ($^\circ$)
ρ	Density (kg/m^3)

Subscripts

abs	Absorbed
dem	Demand
$exch$	Tube exchanger
fl	Fluid
gen	Generated
HEX	Heat Exchanger
inc	Incident
∞	Environment or reference state
ins	Insulation
L	Longitudinal plane
M	Tank material
mw	Makeup Water
sf	Solar field
st	Steam
T	Transversal plane

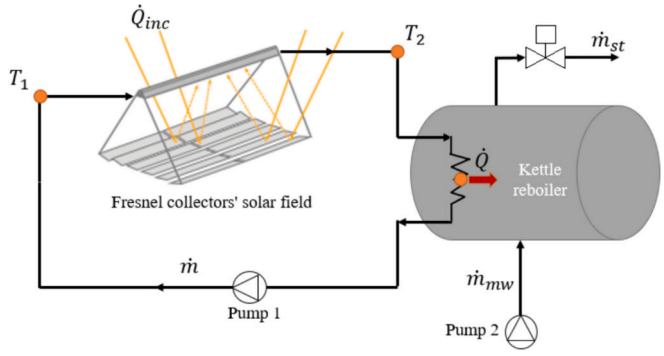

Fig. 1. SHIP system diagram in ISG mode.

Table 1
Linear Fresnel Collector module characteristics and properties.

Property	Value
Aperture Area	26.4 m^2
Optical Efficiency at Normal Incidence Angle	66.7%
Absorber Tube External Diameter	70 mm
Absorber Tube Thickness	2 mm
Glass Cover External Diameter	125 mm
Glass Cover Thickness	3 mm
Heat Transfer Fluid	Pressurised Water
Water Mass Flow	1.65 kg/s
Kettle Reboiler Diameter / Length	600 mm / 2.04 m
Field Orientation	North-South
Field Azimuth	32°
Longitude	39.958°
Latitude	− 0.074°

integration point for a particular operation. For instance, in Ref. [4], the authors conducted a study on flat plate and vacuum tube collectors integrated into an absorption heat transformer for industrial process heat within a temperature range of 80$^\circ C$ to 160$^\circ C$. Furthermore, Valenzuela et al. [5] performed a research study on the integration of a small-scale Concentrated Solar Power (CSP) parabolic trough system to deliver heat

Table 2
Thermal properties of the thermal energy storage material.

Parameter	Value
$C_{p,TES}$	1400 $J/kg \cdot K$
ρ_{TES}	3700 kg/m^3
k_{TES}	2.1 $W/m \cdot K$
Average Rock Diameter	0.02 m
ε	0.4

to the Chilean industrial sector via direct steam generation. Frein et al. [6] presented a model for a SHIP system installed at a pharmaceutical industry, where the simulations results are compared to monitoring data from the SHIP installation. The FRIENDSHIP [7] and SHIP2FAIR [8] projects have demonstrated the potential of SHIP systems to deliver heat for the agro-industrial processes within a medium temperature range of 200$^\circ C$ and 300$^\circ C$. Furthermore, the aforementioned projects have demonstrated the techno-economic feasibility and user-friendliness of the technology.

Although SHIP systems represent a viable option for the decarbonisation of the industry sector, they depend on an intermittent source of energy and are subject to weather conditions. Consequently, a TES system is required to store energy and compensate for the periods when there is no energy resource available. In Ref. [9], the authors analyse the optimal integration of latent TES in solar heating and cooling for an industrial process. The series and parallel coupling of the TES system with dynamic simulations is evaluated, including transient events such as clouds and start-ups. The study concludes that connecting the TES in series represents the optimal configuration for a cost-effective and straightforward solution.

Kanojia et al. [10] discuss the development of packed-bed TES (PBTES) in the context of concentrated solar power (CSP) plants. Seyitini et al. [11] reviewed solid-state sensible TES systems, considering numerical and experimental investigations that evaluated the systems' thermal performance and environmental impact with respect to different design parameters. In Ref. [12], the authors review PBTES systems for low-temperature solar applications based on sensible heat. The analyses are both experimental and numerical, and energy and exergy efficiencies are considered. The authors also discuss the

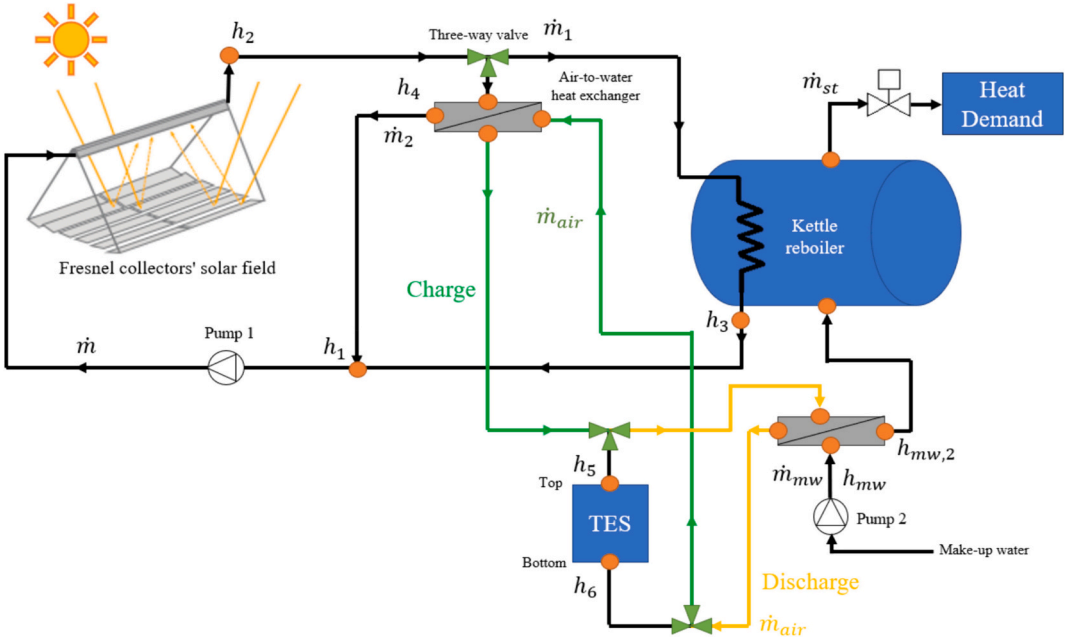

Fig. 2. SHIP and TEs model integration diagram.

Table 3
Control parameters for the storable energy simulation.

Parameter	Value	Unit
Maximum Pressure	8	bar_a
Minimum Pressure	7	bar_a
Maximum Operating Temperature	180	$^{\circ}C$

Table 4
Corresponding storable energy for each solar field size.

Solar field size	Storable energy (*MJ*)
6 modules	342.1
8 modules	986.5
12 modules	2412.2

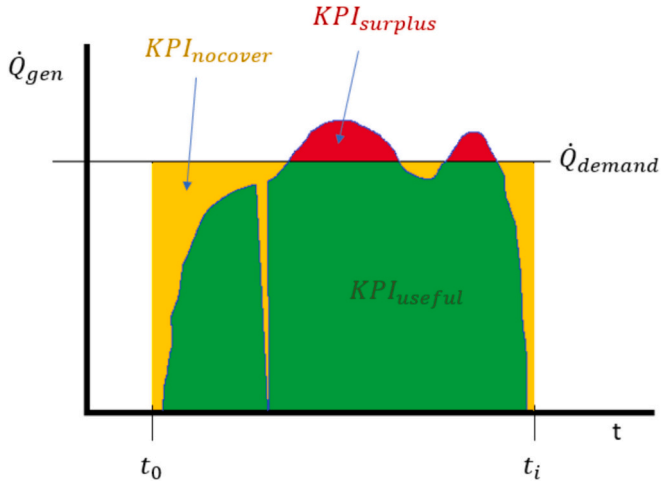

Fig. 3. Graphical example of the key performance indicators.

economic feasibility of these systems and compare them with latent-based systems.

Ref. [13] thoroughly reviews the research on latent-based PBTES considering spherical phase change material encapsulation. The study focuses on optimal design, highlights the applications, and discusses the challenges of such technology. Furthermore, in Ref. [14] the authors experimentally analyse and optimises a cascade latent PBTES system with spherical capsules, offering useful guidance for the design and applications of such systems.

Furthermore, Ref. [15] analyses single- and double-pass PBTES systems, evaluating the impact of bed material and geometrical parameters on the system performance. In Ref. [16], the authors present a laboratory-scale packed-bed cylindrical TES that uses waste materials, which may represent a low-cost and sustainable alternative for TES in SHIP. In Ref. [17], the authors investigate PBTES composed of alumina particles with steam and air as heat transfer fluids. They report experiments with different mass flow rates and discuss their impact on heat transfer and heat loss. Additionally, Ref. [18] uses a quasi-one-dimensional transient model to assess the effect of operational and design parameters on the performance of thermocline PBTES using rocks and high-temperature air. The study reports overall efficiencies above 95% for all cases investigated.

Meanwhile, Ref. [19] explores the thermal performance and economic feasibility of an indirect solar dryer integrated with a PBTES system. The study evaluates the wood drying process through dynamic simulations, demonstrating a reduction in drying time and improved economic feasibility by integrating the TES system. Ref. [20] presents the performance of a solar dryer with a PBTES. The study evaluates the TES potential by focusing on energy consumption and exergy-sustainability indicators, including experiments showcasing operation in off-sunshine hours.

A comprehensive SHIP model is presented that is both simple and precise, allowing for integration with various components. The solar thermal system consists of linear Fresnel solar collectors and a balance of plant that includes a kettle reboiler. The main thermal inertia in the solar thermal model is in the kettle reboiler, which has been dynamically modelled. Additionally, this study also includes a PBTES. Although latent-based TES devices have been drawing attention [21], a sensible PBTES was chosen in this study, seeking to exploit copper slag as filler material. As a byproduct of copper ore processing, besides having a much lower cost than conventional materials used in TES applications,

Table 5
Packed-bed volume as a function of the makeup water temperature and solar field size.

	6 modules	8 modules	12 modules
	m^3		
$V_{@20°C}$	0.5	1.4	3.3
$V_{@45°C}$	1.2	3.4	8.3
$V_{@70°C}$	2.2	6.3	15.3

Table 6
Summary of the parametric study variables.

Parameter			
Solar Field Size	6 modules	8 modules	12 modules
TES Volume (m^3)	0.5	4.7	15.3
Makeup Water Temperature ($^{\circ}C$)	20	45	70
Heat Demand (kW)	70		

copper slag is abundant, readily available, and presents interesting thermophysical properties. Moreover, the modelling for the sensible PBTES used was previously presented in Ref. [22], considering the interactions between the heat transfer fluid and the packed-bed material as a 1-D transient.

This study contributes to the existing literature by presenting an integrated SHIP system for Indirect Steam Generation (ISG) coupled with PBTES system, which allows for the dynamic simulation and in-depth analysis of the system's main variables. Furthermore, the design and performance analysis of a SHIP system coupled with a copper slag PBTES were conducted. The packed-bed model was integrated with the SHIP model to preheat the makeup water of the kettle reboiler. A parametric analysis was performed to design and size the solar field and storage volume. Moreover, two main performance variables (air and makeup water flow rates) were identified as key in the system control and improvements were implemented with respect to said variables. The dynamics and performance of the final integrated system were analysed in depth, showing that proper adjustment of the air mass flow and makeup water flow allows for the system's steady and continuous operation, even on days with low irradiance. Furthermore, a techno-economic analysis was conducted considering the system's size, components, the energy generated, and the resulting savings in natural gas consumption and CO_2 (emissions)

2. Methodology

2.1. SHIP model description

The SHIP system model was developed by creating a set of Differential-Algebraic Equations (DAEs) that represent the physical behaviour of the system's components. MatLab [23] was chosen as the programming environment due to its built-in libraries and solvers for DAE systems. The employed DAE solver is variable-step, thus enabling the time step to be automatically adjusted during the simulation in order to enhance the accuracy of the results. This work presents the modelled SHIP system, which consists of a shell and tube heat exchanger known as a kettle reboiler, a modular Linear Fresnel Collector solar field, a primary circulation pump, a steam extraction valve, and a makeup water pump, as shown in Fig. 1. The SHIP system operates in ISG mode. In Fig. 1, T_1 denotes the inlet temperature of the solar field, and T_2 represents the outlet temperature. The fluid properties throughout the system model were calculated using REFPROP [24].

Thus, the SHIP system is divided into two circuits: the primary circuit, where a heat transfer fluid (HTF) absorbs heat in a close loop through the solar field, and the secondary circuit, which is the steam extraction side. The system is designed to produce heat at medium-range temperatures, i.e., from 150 $^{\circ}C$ to 300 $^{\circ}C$.

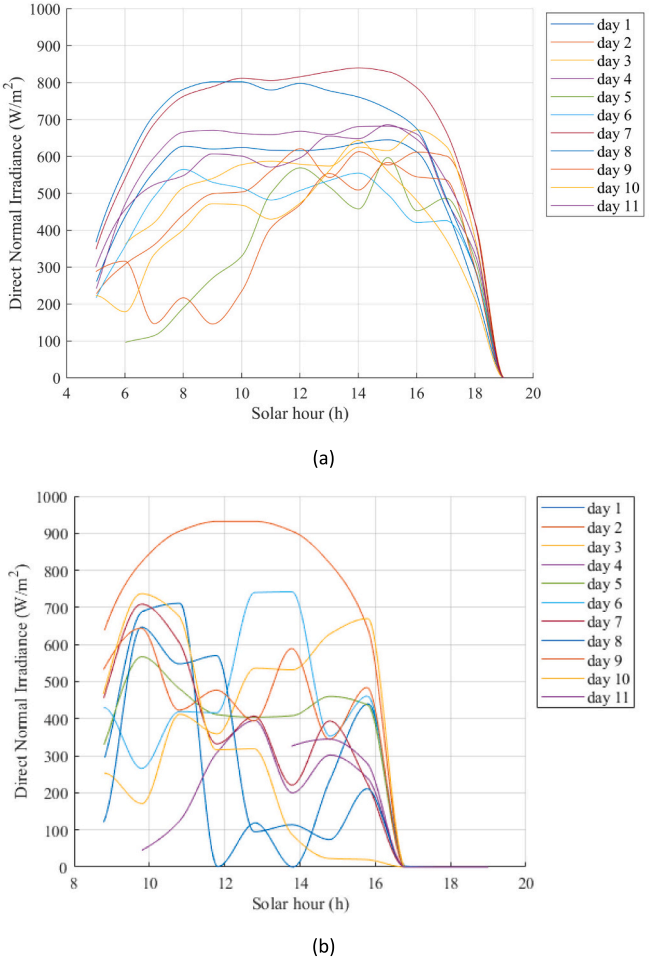

Fig. 4. Direct normal irradiance of the chosen days for the parametric study on summer (a) and winter (b).

2.1.1. Solar field model

The study uses an existing experimental solar field as a reference. The solar field consists of modular linear Fresnel collectors, whose details are specified in Table 1. The aperture area given in Table 1 refers to the area per module. The modularity of the solar collectors allows for flexibility in the design of the solar field and integration into the industrial process.

To calculate the incident heat ($\dot{Q}_{inc}$) on the absorber tube of the solar collectors, an Incidence Angle Modifier (IAM) model was used, taking into account the number of modules (N_{mod}), the aperture area (A), Cl that represents the cleanliness of the reflective surface, and the Direct Normal Irradiance (DNI). [25]The longitudinal and transversal components of the linear Fresnel solar collector are represented in Eq. (1) as IAM_L and IAM_T, respectively, extracted from Ref. [25].

$$\dot{Q}_{inc} = \eta_0 \cdot IAM_L \cdot IAM_T \cdot Cl \cdot A \cdot N_{mod} \cdot DNI \quad (1)$$

The absorber tube's heat losses were computed using Eqs. (2) and (3), which assume a similar behaviour to that of a Eurotrough collector with Schott absorbers [26]. Therefore, the amount of heat lost depends on the DNI incident on the solar field and the length of the absorber tube. It is important to note that θ_{inc} in Eq. (3) represents the solar incident angle. In this study, ΔT was calculated by determining the temperature difference between the inlet temperature of the solar field and the ambient temperature.

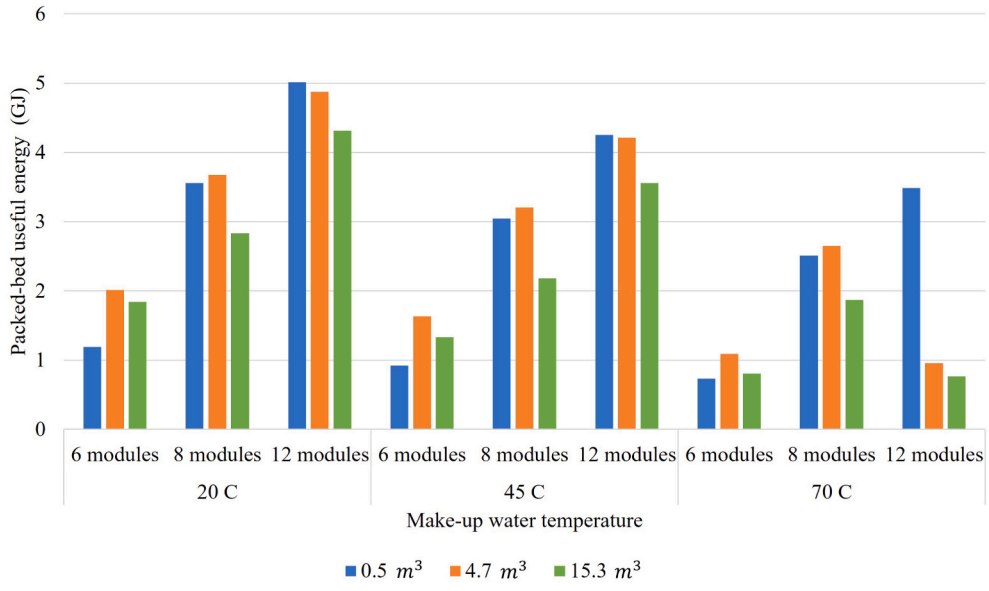

(a)

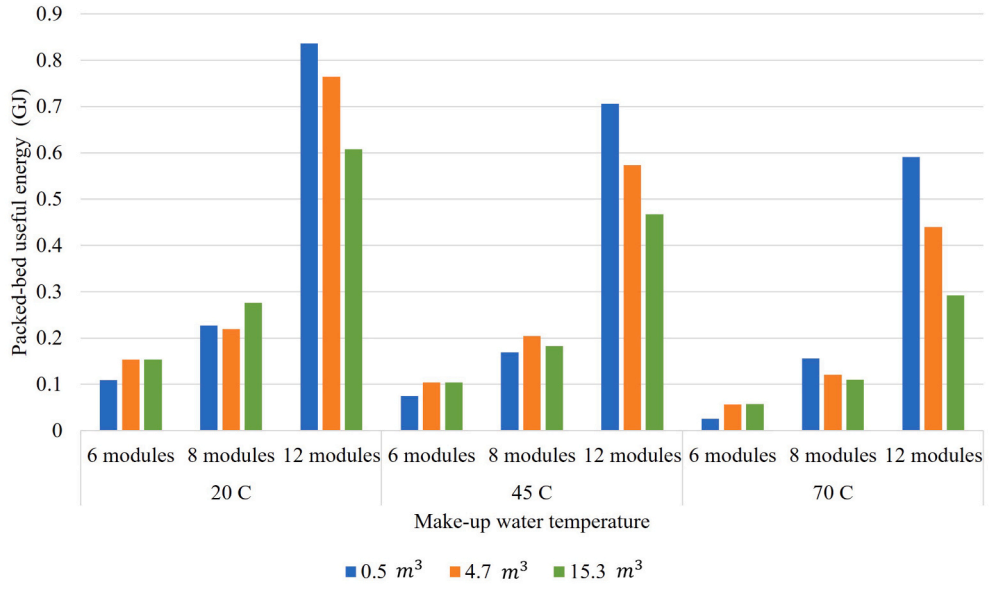

(b)

Fig. 5. Parametric analysis results on the makeup water flow rate and solar field size considering different TES volumes for summer (a) and winter (b).

$$\dot{q}_{loss}\left(\frac{W}{m}\right) = 0.00154\cdot\Delta T^2 + 0.2021\cdot\Delta T - 24.899 + B \tag{2}$$

$$B = \left(0.00036\cdot\Delta T^2 + 0.2029\cdot\Delta T + 24.899\right)\cdot\frac{DNI}{900}\cdot cos(\theta_{inc}) \tag{3}$$

The absorbed heat is then calculated using Eqs. (4) and (5), where l_{sf} represents the length of the solar field in meters.

$$\dot{Q}_{abs} = \dot{Q}_{inc} - \dot{q}_{loss}\cdot l_{sf} \tag{4}$$

$$\dot{Q}_{abs} = \dot{m}\cdot C_p\cdot(T_2 - T_1) \tag{5}$$

2.1.2. Kettle reboiler model

The heat absorbed by the solar collectors, as expressed in Eq. (5), is transferred to the kettle reboiler through a tube heat exchanger inside the tank. The pressure of the tank is maintained at a set level by opening the steam extraction valve located downstream of the kettle reboiler. The liquid water level inside the kettle reboiler is maintained by activating a makeup water pump. The model for the kettle reboiler considers it to be a horizontal cylinder. The two-phase fluid inside the tank is assumed to be in thermodynamic equilibrium at every time step, as studied in Ref. [25]. The properties of the two-phase fluid inside the kettle reboiler are determined by calculating its density (ρ) and specific internal energy (u), taking into account the inertia of the metal mass of the tank (M_M). Eq. (6) represents the variation in density of the two-phase fluid, which is dependent on the inlet and outlet mass flows and the volume of the tank. In Eq. (7), $\dot{Q}_{HEX}$ is defined as the heat transferred from the shell and tube heat exchanger into the fluid inside the kettle

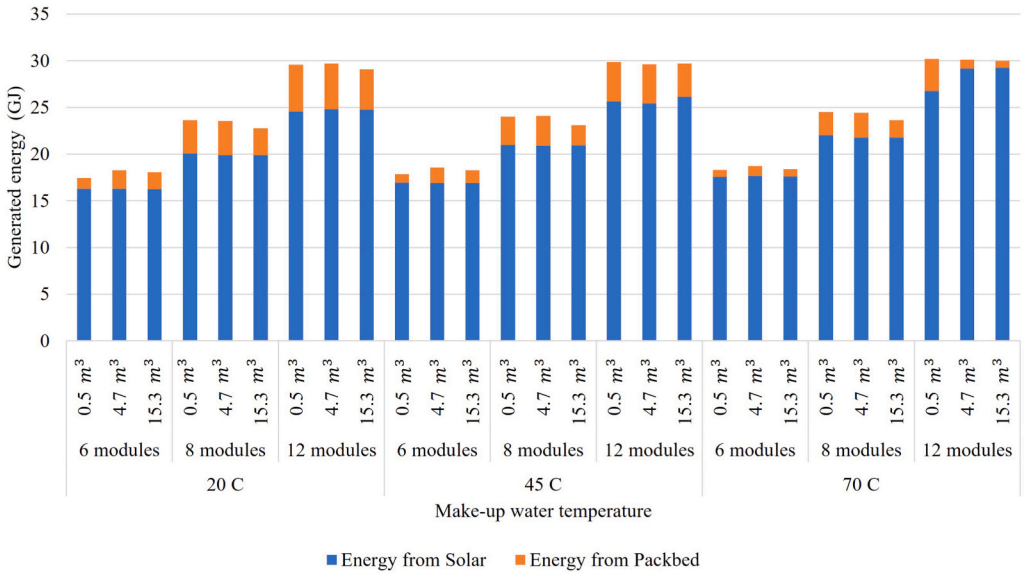

(a)

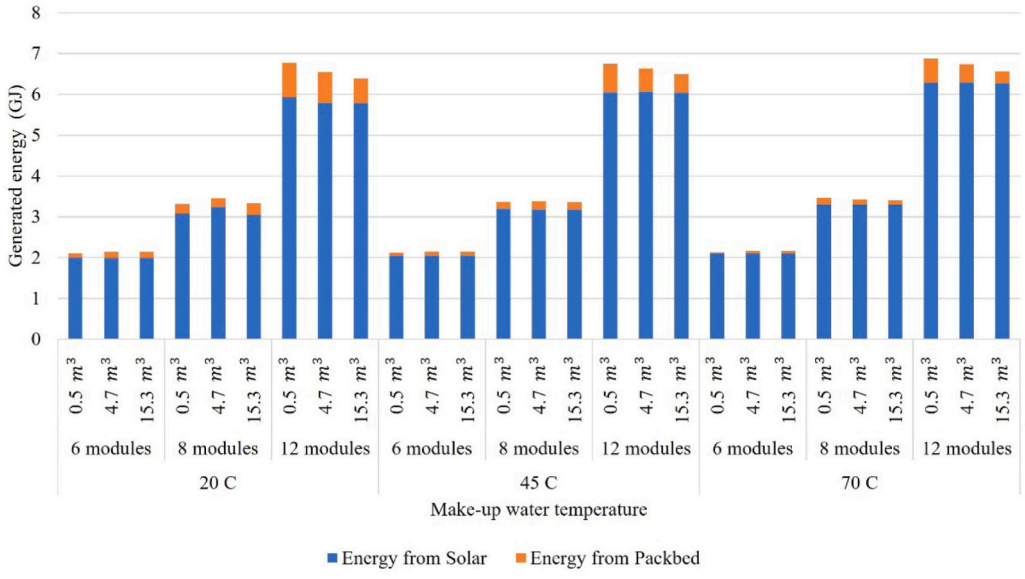

(b)

Fig. 6. Total energy generated by the system divided by the contributions of the solar system and the packed- bed in summer (a) and winter (b).

reboiler, whereas $\dot{Q}_{loss,tank}$ represents the heat loss to the environment along its surface. Eq. (8) represents the total internal energy of the kettle reboiler (E_{tank}), which considers the shares of the two-phase fluid and the metal mass.

$$\frac{d\rho}{dt} = \frac{\sum \dot{m}_{in} - \sum \dot{m}_{out}}{V_{tank}} \tag{6}$$

$$\frac{dE_{tank}}{dt} = \dot{Q}_{HEX} + \sum \left(\dot{m}_{in} \cdot h_{in}\right) - \sum \left(\dot{m}_{out} \cdot h_{out}\right) - \dot{Q}_{loss,tank} \tag{7}$$

$$E_{tank} = \rho \cdot V_{tank} \cdot u + M_M \cdot C_{p,M} \cdot T_M \tag{8}$$

The heat loss of the tank has been modelled employing a one-dimensional heat conduction on a cylinder wall [27].

$\dot{Q}_{HEX}$ is calculated using the effectiveness – NTU method for heat transfer, using the tube heat exchanger model developed in Ref. [28], as presented in Eqs. (9) and (10).

$$\dot{Q}_{HEX} = eff \cdot \dot{m} \cdot C_p \cdot \left(T_{out,solar} - T_{fl}\right) \tag{9}$$

$$T_{out,HEX} = T_{in,solar} = T_{out,solar} - \frac{\dot{Q}_{HEX}}{\dot{m} \cdot C_p} \tag{10}$$

Where T_{fl} is the temperature of the two-phase fluid inside the tank and *eff* is the effectiveness of the tube heat exchanger.

The energy produced by the SHIP system is calculated by integrating the steam mass flow rate and specific enthalpy at the kettle reboiler pressure over a period of time, as demonstrated in Eq. (11).

$$E_{gen} = \int \dot{m}_{st} \cdot h_{st}(P_{tank}) \cdot dt \tag{11}$$

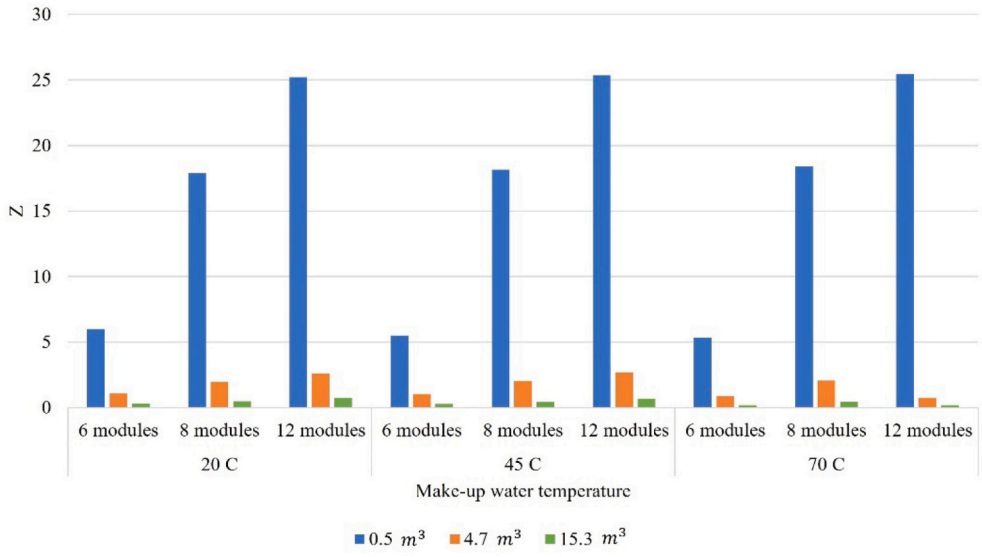

(a)

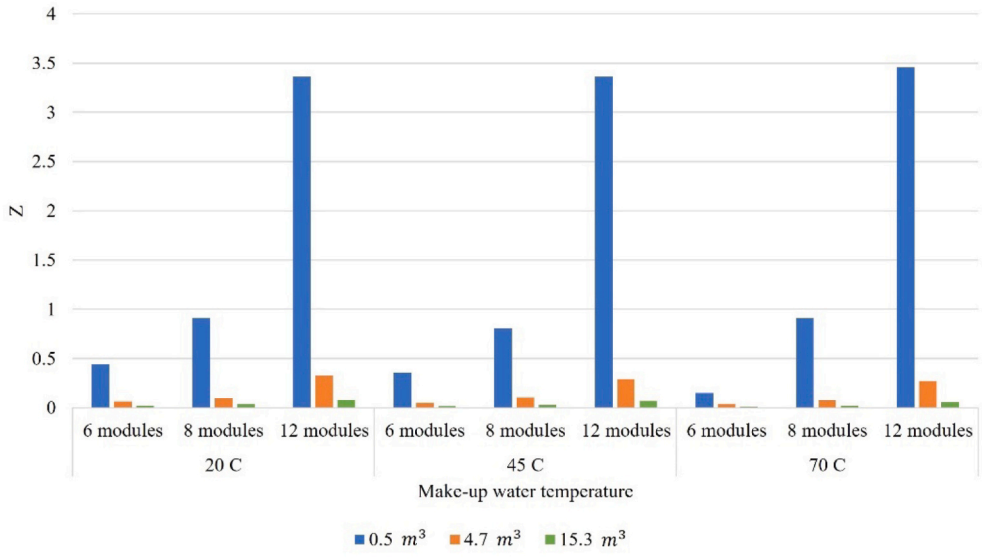

(b)

Fig. 7. Packed-bed utilisation factor. Where the values of Z are shown for: (a) summer cases and (b) the winter cases.

2.2. Thermal energy storage modelling

The thermal energy storage system being considered is a packed-bed of copper slags confined in a cylindrical tank with air as the HTF flowing in the axial direction. The model for the system only considers the development of the thermocline in the axial coordinate and performs energy balances for the fluid and solid phases. The model described by Eqs. (12) and (13) is the continuous solid-phase model proposed by Littman et al. [29], with the addition of a sink term to account for thermal losses in the fluid's energy balance. This formulation is based on the model presented by Calderón-Vásquez and Cardemil (2023) [30], which includes a detailed validation procedure using data from the literature and the correlations for h_v, k_{eff}, and U_w employed in the model. The main assumptions for the continuous solid phase model are listed as follows:

- Plug-flow condition of the fluid flowing through the porous medium.
- Radial thermal conductivity is neglected.
- Uniform temperature on the solid particles.
- Thermal capacitance of the storage insulation is neglected, instead is modelled as a loss term considering an overall heat transfer coefficient between the fluid near the wall and the thermal insulation (U_w).
- The shape of the rocks is assumed spherical and uniform size.
- Void fraction is constant along the porous medium.

$$\varepsilon\left(\rho c_p\right)_{fl}\left(\frac{\partial T_{fl}}{\partial t}+u\frac{\partial T_{fl}}{\partial z}\right)=k_{fl-eff}\frac{\partial^2 T_{fl}}{\partial z^2}-h_v\left(T_{fl}-T_s\right)-U_w A_w\left(T_{fl}-T_\infty\right) \quad (12)$$

$$(1-\varepsilon)\left(\rho c_p\right)_s\frac{\partial T_s}{\partial t}=k_{s-eff}\frac{\partial^2 T_s}{\partial z^2}+h_v\left(T_{fl}-T_s\right) \quad (13)$$

where the subscripts s, f, and ∞ refer to the solid, fluid, and surround-

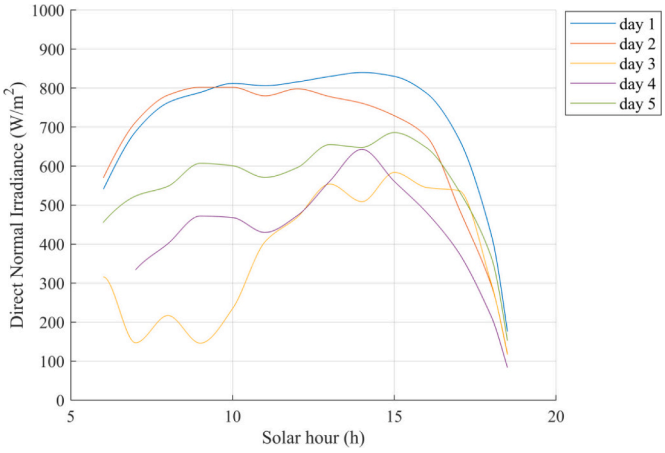

Fig. 8. Daily DNI of the selected days for the analysis.

ings, respectively. The temperature T is a function of time t and the axial coordinate of the TES z. The void fraction of the porous medium, ε, is assumed to be uniform along the packed-bed. The density, thermal capacity, and effective thermal conductivity of the phases are represented by ρ, c_p, and k_{eff}, respectively. The volumetric heat transfer coefficient h_v models the convective heat transfer caused by the temperature difference between fluid and solid. The interstitial fluid moving at velocity is represented by u. Thermal losses to the surroundings are modelled through the overall heat transfer coefficient U_w with a specific contact area a_w between the fluid and the storage walls.

The Method of Lines (MOL) is used to solve the system of Partial Differential Equations (PDEs). The Finite Differences Method is used for derivatives with respect to z, resulting in $2N_z$ linear ODEs. The ODEs are then integrated using the *solve_ivp* function from the optimization subpackage of SciPy [31], programmed in Python [32].

The properties of the copper slag used in this study, reported in Ref. [22], are displayed in Table 2.

2.3. Integrated system description

The copper-slag-PBTES has been implemented to preheat the makeup water of the kettle reboiler. This water could be low-temperature water from processes condensate or from the water main. The integration scheme was chosen because it is the point in the system where there is a higher temperature difference. The integrated system consists of two air-to-water heat exchangers that facilitates the charge and discharge of the packed-bed. Air has been selected as the HTF for the packed-bed. One heat exchanger is positioned at the solar field outlet while the other is located after the makeup water pump.

The TES model was integrated into the SHIP system model using the compatibility between Python and MatLab. Fig. 2 shows the diagram of the integrated system model.

2.3.1. System operation and control

The integration method chosen for this system involves two air-to-water heat exchangers as shown in grey in Fig. 2. The system operates in three modes: normal, charge, and discharge. During normal mode, the total water flow runs through the heat exchanger inside the kettle reboiler with a mass flow rate of $\dot{m}_1 = \dot{m}$, thus transferring all the useful heat absorbed in the Linear Fresnel solar field. The packed-bed remains idle during normal mode.

During the charging mode, the pressurised water leaving the solar field is split into two streams: $\dot{m}_1$ enters the heat exchanger inside the tank and $\dot{m}_2$ passes through the air-to-water heat exchanger. The flow leaving the kettle reboiler and the flow after the air-to-water heat exchanger are mixed before entering the Linear Fresnel solar field, resulting in $\dot{m} = \dot{m}_1 + \dot{m}_2$. The division of the flow is controlled by the instantaneous heat generated. This ensures that the heat flow remains below the maximum thermal power ($\dot{Q}_{dem}$), which is determined by the heat demand, and the packed-bed stores the thermal energy surplus. Furthermore, an energy balance is performed to calculate the specific enthalpy of water at the inlet of the solar field (i.e., h_1) as:

$$\dot{m} \cdot h_1 = \dot{m}_2 \cdot h_4 + \dot{m}_1 \cdot h_3 \tag{14}$$

In addition, air enters the heat exchanger with a mass flow rate of $\dot{m}_{air}$ and specific enthalpy of h_6, as shown in Fig. 2, and exchanges heat with water with specific enthalpy of h_2 and mass flow rate of $\dot{m}_2$. The air exits the heat exchanger with a specific enthalpy of h_5 and enters through the top side of the packed-bed to charge the TES device.

Fig. 2 shows that air flows from the bottom to the top of the packed-bed during discharge mode, and the heat transfer fluid preheats the makeup water. The packed-bed discharges when the liquid inside the tank reaches a minimum level (when pump #2 activates). Makeup water flows through the heat exchanger during packed-bed discharge, absorbing the heat from the air and increasing its temperature. In this mode, the mass flow rate in the solar field is $\dot{m}_1 = \dot{m}$, and the useful heat absorbed in the solar field is introduced into the kettle reboiler.

The air heat exchanger has been modelled using the effectiveness – NTU method [27] for calculating heat transfer between the air and the water. The water and air temperatures are introduced as inputs, and the minimum heat capacity rate, C_{min}, between both flows is calculated in each time step. With this information, the heat transfer is calculated as.

$$\dot{Q}_{exch} = eff_{exch} \cdot C_{min} \cdot (T_{high} - T_{low}) \begin{cases} charge: C_{min} = min\left(\dot{m}_2 \cdot C_{p,2}, \dot{m}_{air} \cdot C_{p,air}\right) \\ discharge: C_{min} = min\left(\dot{m}_{mw} \cdot C_{p,mw}, \dot{m}_{air} \cdot C_{p,air}\right) \end{cases} \tag{15}$$

and the model outputs the outlet temperature of both fluids from the heat exchanger.

2.4. System design

The volume of the packed-bed and the size of the solar field have been chosen as parameters to design the SHIP system. The solar field size determines the amount of energy that can be stored in the TES. This is calculated by integrating the generated energy throughout the day when it exceeds the required heat demand (i.e., the thermal energy surplus) as:

$$E_{storable} = \int \left(\dot{Q}_{gen} - \dot{Q}_{dem}\right) \cdot dt, if\ \dot{Q}_{gen} > \dot{Q}_{dem} \tag{16}$$

where $\dot{Q}_{dem}$ refers to the established heat demand. The storable energy is calculated utilising the SHIP model considering that:

- all the absorbed heat is transferred into the kettle reboiler.
- steam is generated if the tank's pressure is between the control pressure limits.

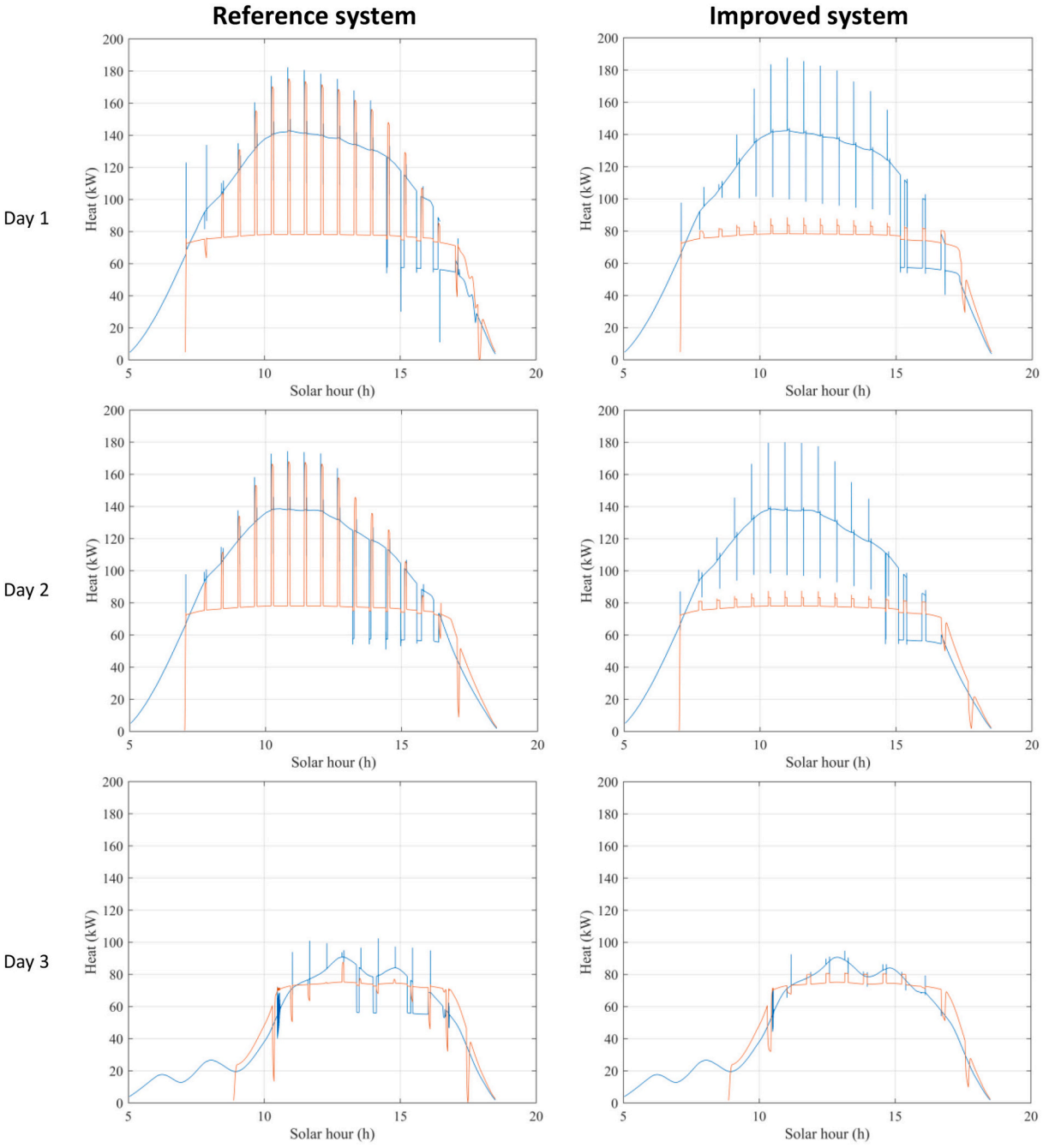

Fig. 9. Absorbed and generated heat by the SHIP and packed-bed system for the reference and the improved system.

The required volume of the TES is then estimated using the storable energy employing Eq. (17).

$$V_{TES} = \frac{E_{storable}}{\rho_{TES} \cdot C_{p,TES} \cdot (1-\varepsilon) \cdot (T_{max} - T_{mw}) \cdot \eta} \tag{17}$$

The maximum operating temperature of the system for normal operating conditions, and the makeup water temperature are represented by T_{max} and T_{mw}, respectively. ρ_{TES} represents the density and $C_{p,TES}$ the thermal capacity of the filler material. Furthermore, a storage efficiency of $\eta = 0.8$ [30] was used to estimate the packed-bed volume. The diameter of the TES has been estimated based on the aspect ratio of the diameter and height of the vessel of $AR = H_{TES}/D_{TES} = 1$ [22].

This study analyses the viability of various TES volumes and solar field sizes. Indicators have been established to calculate the energy generated by the system, the useful energy delivered by the packed-bed, and the energy storage utilisation for each system size.

The useful energy is described as the energy extracted during the TES discharge; hence, it is a function of the specific enthalpy difference of the air flowing from the top to bottom of the packed-bed integrated throughout the analysed period, as shown in Eq. (18).

$$E_{useful} = \int \dot{m}_{air} \cdot (h_5 - h_6) \cdot dt \tag{18}$$

A variable that quantifies the utilisation of the packed-bed for each system size has been introduced to choose the optimum volume of the energy storage system. The utilisation factor Z, described in Eq. (19), is the ratio of the useful energy delivered by the TES and its designed store capacity.

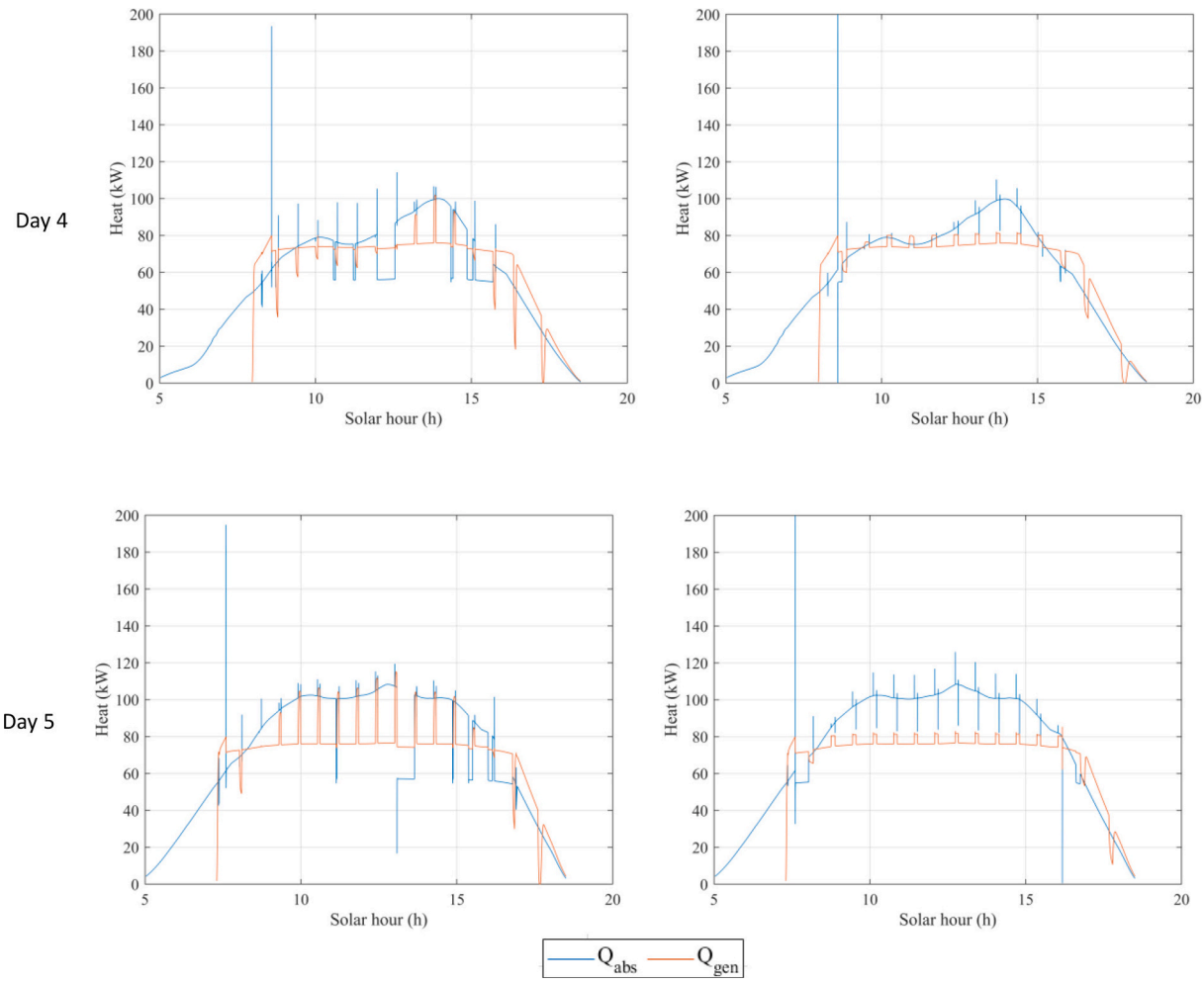

Fig. 9. (*continued*).

$$Z = \frac{E_{useful}}{\rho_{TES} \cdot V_{TES} \cdot C_{p,TES} \cdot (1-\varepsilon) \cdot (T_{max} - T_{mw}) \cdot \eta} \tag{19}$$

Consequently, the factor Z represents a quantification of the utilisation of the packed-bed throughout the operational period for each system size. This means the number of complete charge/discharge cycles.

2.4.1. Parametric study

This study conducts a parametric analysis to investigate the impact of the TES volume on the corresponding solar field size. The goal is to determine the most suitable TES volume for a given solar field size. Table 3 displays the control parameters used. Simulations were carried out for typical summer and winter days under clear-sky conditions. Consecutive days were chosen to allow the development of charge and discharge hysteresis to the packed-bed. Furthermore, the weather conditions data for the model was obtained using a TMY file of the solar field location.

2.5. Dynamic analysis and operation improvement

After analysing the parametric study results and selecting the system size, the corresponding control parameters are used to simulate the system. The dynamic operation of the system is then analysed, and system variables are adjusted to improve its behaviour and meet the heat demand without overproducing energy. The proposed operating variables for modification are the TES circuit's air mass flow rate and the makeup water volumetric flow.

2.5.1. Key performance indicators

Key performance indicators (KPIs) are proposed to further understand the behaviour of the system. The KPI described in Eq. (20) is related to the surplus of heat generation. Moreover, a KPI that quantifies the amount of energy demand that is not covered by the system during the operating period is shown in Eq. (21). Eq. (22) describes a KPI that quantifies the energy generated relative to the total energy demand for the operating period. Additionally, the total useful energy generated below the heat demand limit is also considered a KPI (Eq. (23)), as illustrated in Fig. 3.

$$KPI_{surplus} = \int_{t_0}^{t_i} \dot{Q}_{gen} \cdot dt, \; if \; \dot{Q}_{gen} > \dot{Q}_{dem} \tag{20}$$

$$KPI_{nocover} = E_{dem} - \left(E_{gen} - E_{exc}\right) \tag{21}$$

$$KPI_{dem} = \int_{t_0}^{t_i} \left(\dot{Q}_{gen} - \dot{Q}_{dem}\right) \cdot dt \tag{22}$$

$$KPI_{useful} = E_{gen} - E_{exc} \tag{23}$$

2.6. System cost

To conduct the economic analysis of the SHIP with packed-bed model, certain assumptions were made.

The cost of the Linear Fresnel collar field was assumed to be $300€/m^2$ [33]. Furthermore, the analysis includes the cost of the TES system, which takes account of the construction materials, i.e. the material of the

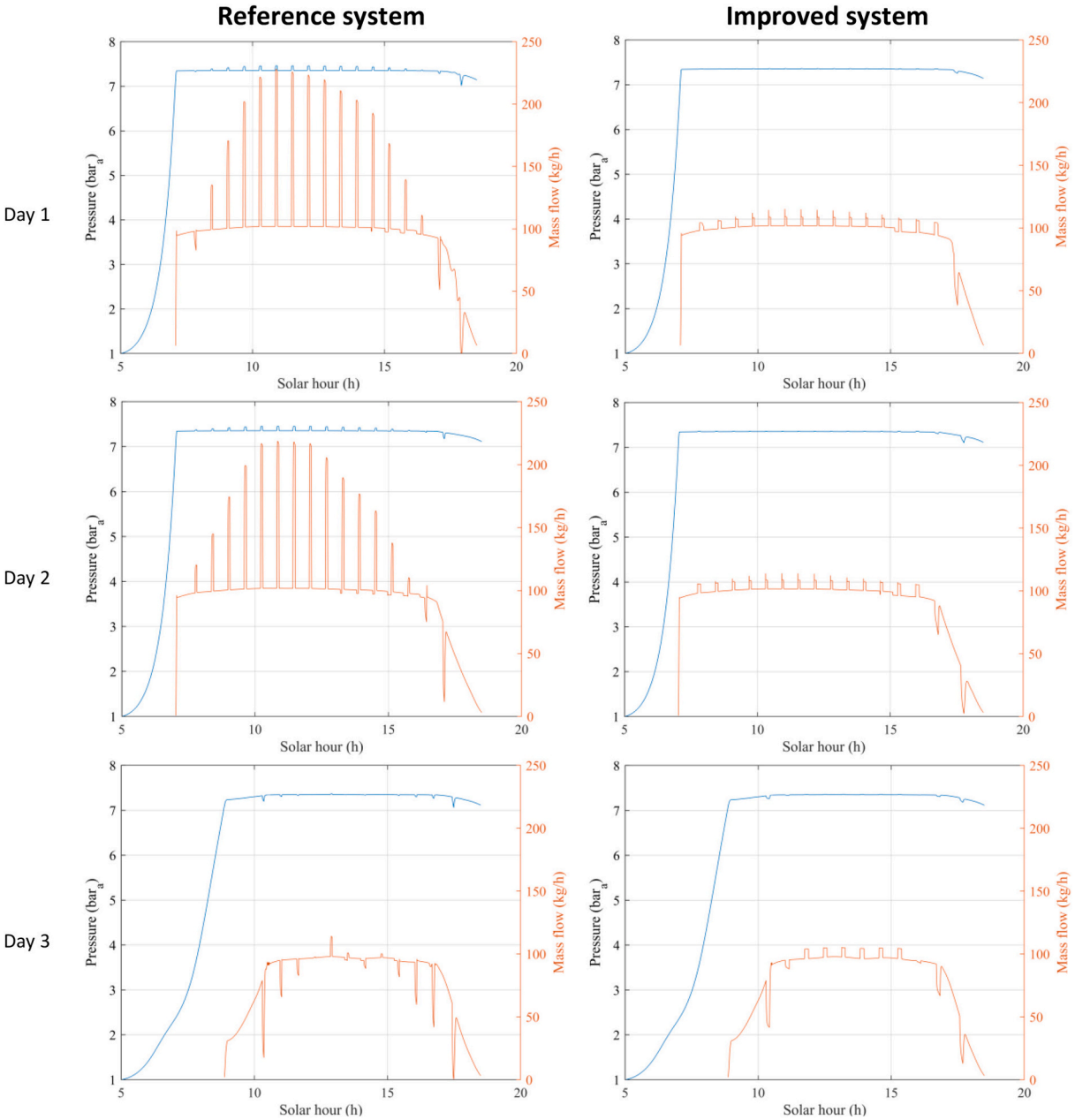

Fig. 10. Pressure of the kettle reboiler and extracted steam mass flow for the reference (a) and the improved (b) system.

tank and its insulation. The cost of the copper slag is disregarded in this study, since it is a waste material, and its potential use is still being investigated. Therefore, the cost of the packed bed is calculated as outlined in Ref. [30] as:

$$C_{TES} = C_{steel} \cdot \rho_{steel} \cdot V_{steel} + C_{ins} \cdot V_{ins} \tag{24}$$

where $C_{steel} = 1.126\ €/kg$, which is the average specific cost of hot rolled plate steel from November 2022 to September 2023, obtained from the world steel prices [34]. The density of steel, ρ_{steel}, is 7850 kg/m^3 [27]. V_{steel}represents the total steel volume required to build the TES tank, and is calculated based on the diameter of the TES and the wall thickness, s_{steel}, which can be calculated with the following expression [35]:

$$s_{steel} = \frac{P_{air} \cdot (D_{TES} + 2 \cdot s_{ins})}{2 \cdot (\sigma_{steel} - 0.5 \cdot P_{air})} \tag{25}$$

where P_{air} is the air pressure, σ_{steel} is the yield strength of steel of 140 *MPa* [35], and s_{ins} refers to the insulation thickness of 55 *mm*, which is based on a reference TES tank installed at a solar thermal laboratory of the *Instituto de Ingeniería Energética* (IIE-UPV).

The insulation cost, defined as C_{ins} in Eq. (24), is the volumetric cost of the insulation material. Microtherm was chosen as the insulation material for this study. According to Ref. [36], the volumetric cost of Microtherm in 2018 was 4269 $\$/m^3$. However, using Eq. (26) [37] and the CEPCI index [38], an estimated actual price for the material can be calculated. In Eq. (26) I is the CEPCI index for the corresponding year, in which $I_{2018} = 603.1$ and the preliminary value on November 2023 was $I_{2023} = 789.2$. Therefore, the cost of insulation in 2023 is 5158.4 $€/m^3$, calculated using the conversion rate of 0.923 €/$ at the time of writing.

$$C_{ins,2023} = C_{ins,2018} \cdot \left(\frac{I_{2023}}{I_{2018}} \right) \tag{26}$$

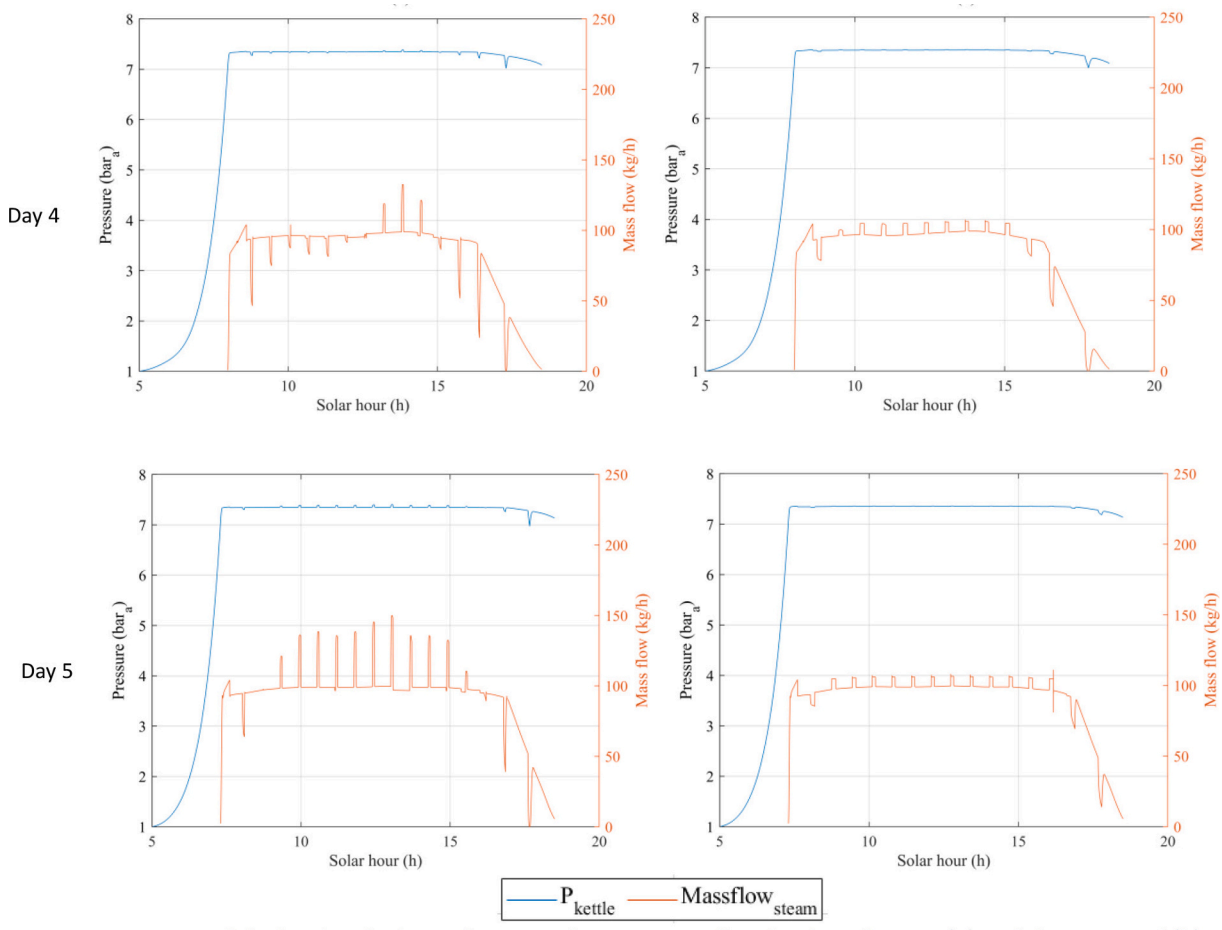

Fig. 10. (*continued*).

The study presents the SHIP and TES system, which requires two air-to-water heat exchangers. The specific cost of these heat exchangers has been assumed to be $c_{exch} = 120\ €/kW$ [39]. Therefore, the cost of the heat exchangers is calculated as follows:

$$C_{exch} = 2.\frac{E_{storable}}{t_{ch/dch}}.c_{exch} \tag{27}$$

The energy stored by the TES, $E_{storable}$, can be calculated employing Eq. (17). The time required for a charge/discharge cycle ($t_{ch/dch}$) was estimated using the dynamic analysis of the system. Additionally, to incorporate the cost of the fan in the analysis, it is assumed that its cost is 10% of the cost of the heat exchangers.

3. System design

3.1. Design parameters

A parametric study is performed using the collector and tank characteristics described in Table 1. The study employed a number of control variables, including the size of the solar field and the volume of the packed-bed vessel. Furthermore, the study analysed the effect of three different makeup water temperature levels: 30°C, 45°C, and 70°C.

The SHIP model was employed to estimate the potential storable energy for the different solar field sizes, which were calculated according to Eq. (16). The selected solar field sizes and their respective potential storable energy are presented in Table 4. These estimates were derived by utilising a proposed heat demand of 70 kW. Therefore, the potential storable energy represents the energy generated above the heat demand.

Consequently, the TES volume can be estimated using Eq. (17) for each proposed makeup water temperature level and storable energy. This yields nine different TES volumes, which are presented in Table 5. In order to limit the dimension of the study, the maximum, the minimum, and average value of the nine volumes (4.7 m^3) were chosen to be used for each case to be analysed.

The variables that were modified throughout the parametric study and their proposed values for each solar field size are presented in Table 6. Consequently, a total of 27 simulation cases were analysed, comprising three solar field sizes with three TES volumes and three makeup water temperatures for each size.

The parametric study was performed for a typical summer and winter 11 consecutive days, including high and low irradiance days. The days were selected as continuous days with clear-sky and cloudy irradiance profile, which could be comparable. Additionally, the simulation was conducted utilising weather data extracted from a TMY data sourced from Valencia, Spain obtained from Meteonorm [40], which comprises hourly data spanning a 365-day year. Consequently, required input data between hours is dynamically interpolated by the solver.

Fig. 4 (a) and (b) show the Direct Normal Irradiance (DNI) profiles obtained from the TMY data of the summer and winter days, respectively. The DNI profiles depicted in Fig. 4 (a) pertain to the month of June, where day 1 corresponds to the 3 of June, whereas those depicted in Fig. 4 (b) pertain to the month of January, where day 1 corresponds to the 20 of January.

The use of consecutive days allows the packed-bed thermocline to have enough charge and discharge cycles to achieve its representative operating conditions.

A detailed study was conducted on the parametric results regarding

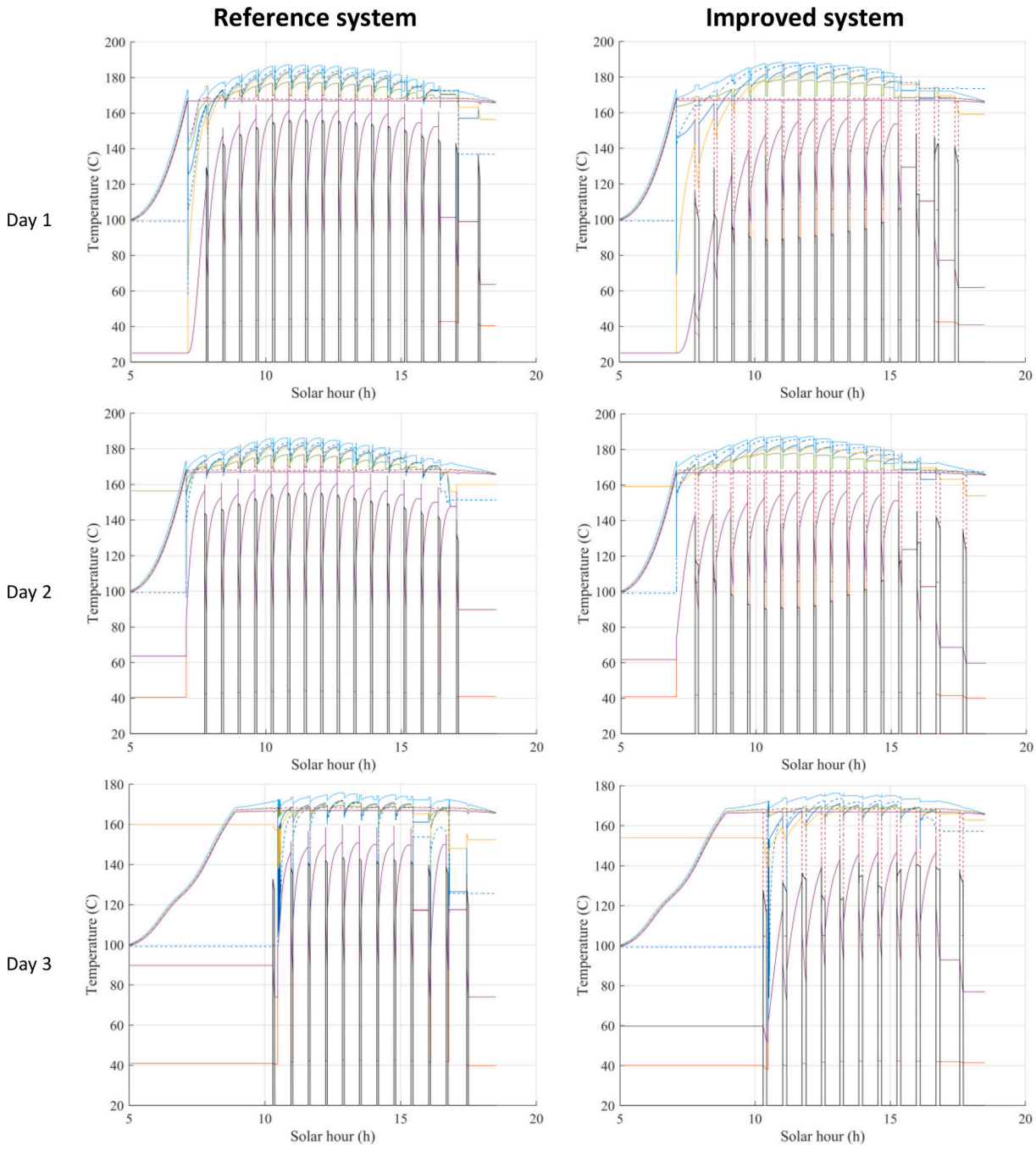

Fig. 11. Temperatures in the solar field, air, packed-bed, makeup water, and the kettle reboiler for the reference (a) and the improved (b) system.

the useful energy that the packed-bed is able to provide to the system. During the parametric study, the packed-bed was charged as long as there was absorbed heat higher than the assumed heat demand, and the discharge occurred when the makeup water pump was active.

3.2. Parametric study analysis

Fig. 5 displays the total useful energy produced for each solar field size in both summer and winter cases. In Fig. 5 (a) (i.e., summer case), it is observed that the greater the TES volume is, the less energy can be used from the packed-bed. This is because the energy that is injected into the packed-bed is distributed into more mass; thus, the temperature of the material does not increase with the same energy provided by the solar thermal system. The same situation occurs in the winter case, as shown in Fig. 5 (b). Although it would seem that the storage volume of 4.7 m^3 is the best size, as the makeup water temperature increases, it is clear that the storage volume of 0.5 m^3 is best utilised in terms of the energy it can deliver.

The difference between the useful energy of volumes 4.7 m^3 and 0.5 m^3 is not different in the case of the 12-module solar field, with makeup water temperatures of 20$^{\circ}C$ and 40$^{\circ}C$. However, this also means that higher volumes may be oversized for the solar field sizes proposed in the parametric analysis, as seen in the results of the energy provided by the packed-bed with a volume of 15.3 m^3.

Fig. 6 shows the amount of energy provided by the SHIP system and by the packed-bed into the final energy generated for each case. During

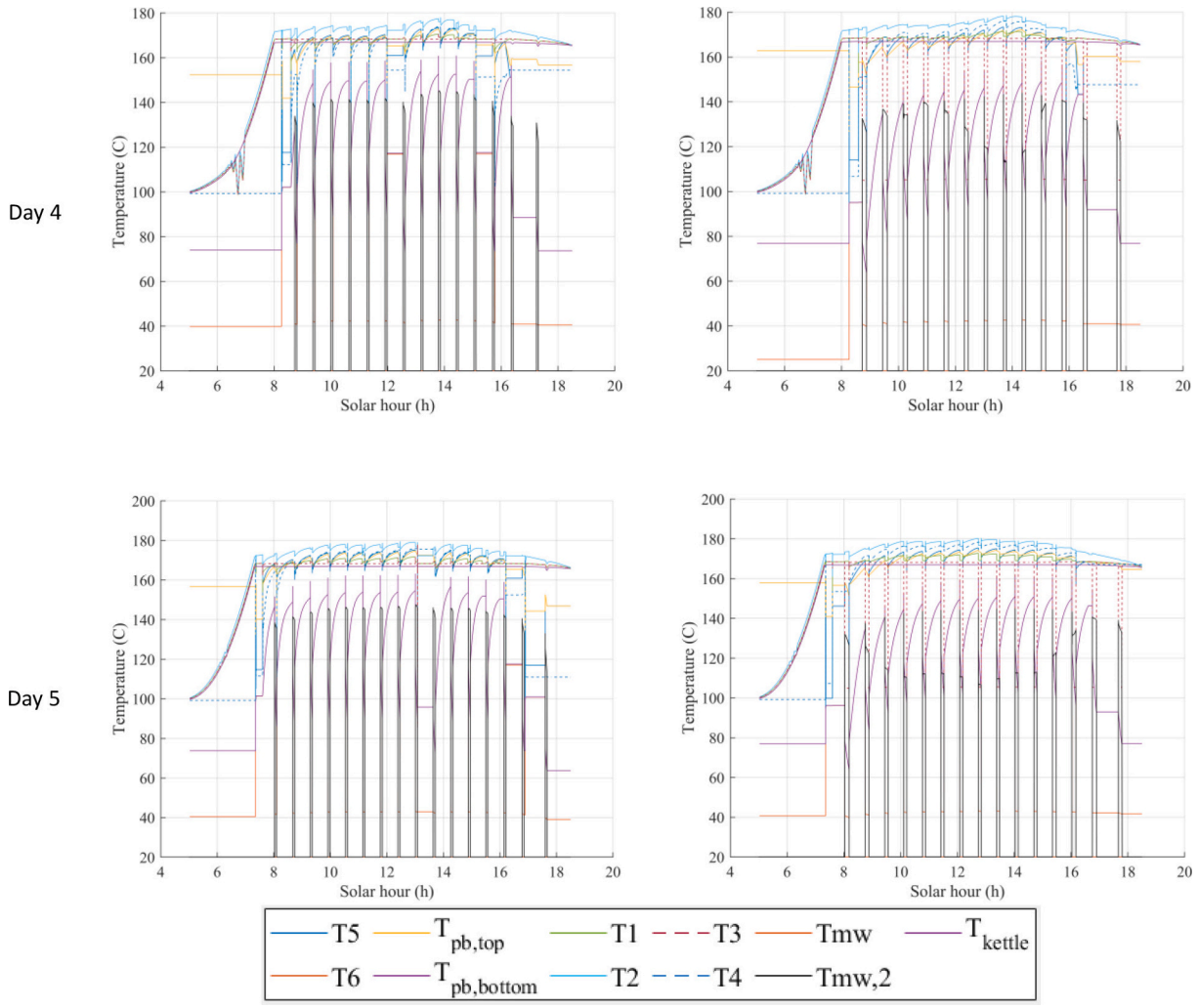

Fig. 11. (*continued*).

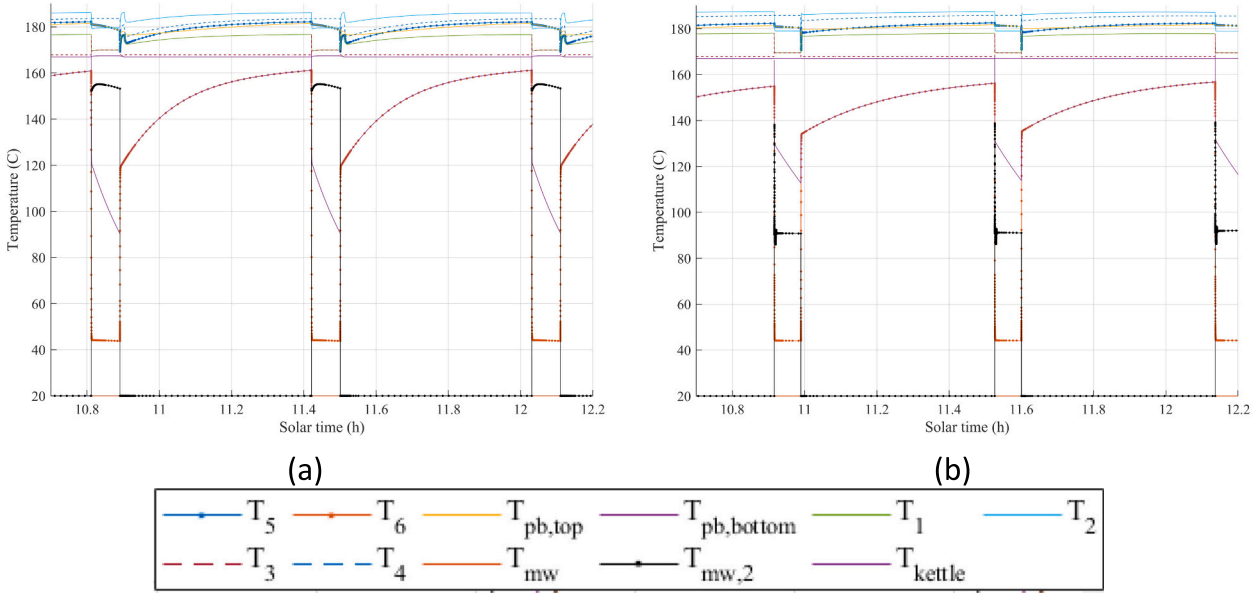

Fig. 12. Detailed view of the temperature in the solar field, air, packed-bed, makeup water, and the kettle reboiler of the (a) reference system and (b) improved system.

Table 7
System parameters.

Component	Parameter	Value	Unit
Fresnel collector	Rows	2	–
	Collectors per row	6	–
Heat exchanger	Effectiveness	0.85	–
Packed-bed	Volume	0.5	m^3
	Initial temperature	25	$^{\circ}C$
Air	Mass flow	1	kg/s
	Pressure	1	bar_a
Control	Maximum pressure	8	bar_a
	Minimum pressure	7	bar_a
	Heat demand	80	kW
	Operating time	16	h
Makeup water	Temperature	20	$^{\circ}C$

summer, the considered volumes deliver similar amounts of energy for all solar field sizes except when the makeup water temperature is 70 $^{\circ}C$. However, during winter, the 0.5 m^3 volume is beneficial in the 12-module system since more heat can be harnessed from the packed-bed.

Fig. 6 shows that the energy harnessed from the packed-bed is similar in each volume and solar field size. However, because one may observe that this metric is not sufficient to determine the suitable TES volume and solar field size, the parameter Z is calculated for each case. Fig. 7 presents the utilisation factor Z for each solar field size and TES storage volume considering summer and winter days. As observed, the storage volumes 4.7 m^3 and 15.3 m^3 both lead to Z values noticeable lower than the volume of 0.5 m^3 on both summer and winter cases. This means that 4.7 m^3 and 15.3 m^3 are over dimensioned volumes for the proposed solar field with the studied makeup water temperatures. Moreover, the 12-module solar field uses more the TES than the other two solar field sizes and utilises the packed-bed around three times more in winter. Therefore, the chosen system is a solar thermal field with 12 modules coupled with a PBTES of 0.5 m^3.

To summarize the results of the parametric study, the combination of the 12-module linear Fresnel solar field with a PBTES of 0.5 m^3 was selected due to the following reasons:

- The energy generated with 12 modules is higher than the cases with a lower number of modules.
- In winter, the system generates more energy with 0.5 m^3 of TES, while in summer the energy generated is similar with the three TES volume sizes. Furthermore, a smaller TES volume reduces the system costs.
- This combination delivers the highest utilisation factor in all the simulated cases. Consequently, more useful energy is extracted in each charge/discharge cycle.
- The oversizing of the solar field allows for the excess heat generated to be stored and subsequently utilised when solar resource is lacking.

Table 10
KPIs of the SHIP system without the packed-bed TES.

Day	Energy generated (MJ)	$KPI_{nocover}$ (MJ)	KPI_{dem} (MJ)
1	2529	1068	−1351
2	2479	1120	−1403
3	1754	1845	−2128
4	2030	1571	−1854
5	2363	1238	−1522
∑	11,154	6842	−8258

4. Dynamic analysis of the system

A simulation of five consecutive typical summer days was performed to analyse the system dynamics. The analysis includes charging from ambient temperature to operating temperature. The heat from the solar field is transferred into the kettle reboiler when makeup water is introduced into the tank, and the solar collectors defocus when the packed-bed is fully charged. The analysis considers the heat exchanger effectiveness to be constant and based on an existing air-to-water heat exchanger installed at a solar thermal laboratory of the *Instituto de Ingeniería Energética* (IIE-UPV). The heat exchanger's proposed effectiveness falls within the expected range for these devices.

The table below presents the reference parameters for the simulation. The parameter *operating time* refers to the duration of sunlight: the total energy demand for this period is calculated using the specified time period.

Fig. 8 illustrates the daily DNI for the selected days used in the simulations. Days with both high and low irradiance were selected to capture the dynamics of the packed-bed operation during charge and discharge as well as the storage thermocline. Furthermore, the chosen system size is simulated with all components and initial conditions.

4.1. Improved system description

The parameters controlling the air mass flow rate and the makeup water flow were adjusted to enhance system performance and reduce energy waste. A linear control was implemented for the makeup water, reducing the flow when heat generation is below the heat demand and

Table 8
Reference system.

Day	Energy generated (MJ)	$KPI_{surplus}$ (MJ)	KPI_{useful} (MJ)	$KPI_{nocover}$ (MJ)	KPI_{dem} (MJ)
1	3192	243	2948	649	−689
2	3089	206	2883	715	−793
3	2078	2	2077	1523	−1804
4	2418	10	2408	1192	−1465
5	2835	57	2778	823	−1049
∑	13,612	518	13,094	4902	−5800

Table 9
Improved system.

Day	Energy generated (MJ)	$KPI_{surplus}$ (MJ)	KPI_{useful} (MJ)	$KPI_{nocover}$ (MJ)	KPI_{dem} (MJ)
1	2969	11	2958	639	−912
2	2888	10	2877	721	−994
3	2107	1	2106	1493	−1775
4	2450	2	2448	1152	−1433
5	2805	6	2799	802	−1080
∑	13,218	30	13,189	4807	−6194

Table 11
Mass of the filler material and wall thickness of the PBTES for the select volume.

PBTES volume (m^3)	Storage mass (kg)	Wall thickness (mm)
0.5	1850	0.35

Table 12
Annual analysis: Energy demand, gas consumption, and Cost.

Parameter (Annual)	Value	Unit
Energy demand	467.2	*MWh*
Natural Gas consumption	519.1	*MWh*
Cost of natural gas	41,528.9	€

Table 13
Comparison between the system with and without the TES: Energy generation, gas savings, and investment cost.

Parameter	Without TES	With TES	Unit
Annual energy generation	111.56	119.62	*MWh*
Gas savings	9916.9	10,633.3	€
Total investment cost	95,040	120,041.4	€
Payback period	12	14	*years*
Saved CO_2 emissions	28.1	30.1	*t* CO_2

increasing it when the maximum heat demand limit is reached. This prevents a drop in the kettle reboiler pressure and consequent reduction in the steam flow. However, the tank's pressure can also be decreased to reduce the peaks observed in the previous section. Additionally, the air mass flow rate was reduced from 1 kg/s to 0.5 kg/s.

4.2. Analysis results

Fig. 9 illustrate the daily heat absorbed by the solar collectors and the heat generated by the SHIP system for both the reference system and the improved system. In the reference system, the generated heat remains within the heat demand limits, but peaks occur when the makeup water pump is activated. This is due to the energy carried by the makeup water transferred along with the heat from the solar field. During the operating period, the absorbed heat decreases at certain points in the simulation due to the defocusing of the solar collectors when the storage is fully charged.

Fig. 9 illustrates the significant reduction in heat generation peaks achieved by the implemented measures in the improved system. Additionally, on days with low irradiance, the heat generated is more consistent, with drops only observed during the last hours of sunlight. Fig. 9 also indicates the moments when the solar collectors defocus. In contrast to the reference system, the solar collectors remain focused even during days with low irradiance. It is important to note that the peaks in the absorbed heat, as observed in Fig. 9, are instantaneous numerical singularities caused by the rapid change of the system between operating modes.

The makeup water and the heat from the solar field increase the pressure inside the kettle reboiler, as shown in Fig. 10. The model calculates the corresponding steam mass flow rate to be at equilibrium, aiming at maintaining a constant pressure. Each time the pressure is modified, the model reaches the equilibrium with a higher steam mass flow rate. However, on days with low irradiance, heat-generated peaks are lower than those with high irradiance. Furthermore, during periods of low irradiance, the introduction of makeup water decreases the steam mass flow rate in contrast to days with high irradiance. The pressure rises because there is sufficient heat transfer to the makeup water. Also, although venting excess heat generated (i.e., above the heat demand limit) is not ideal it is necessary to prevent overpressure in the process feed system.

By implementing control and adjustment of operating values, the pressure inside the kettle reboiler remains constant throughout the operating period, even on days with low irradiance, as shown in Fig. 10. Consistency in the pressure of the tank is crucial to maintain a steady pressure in the customer steam line. Moreover, the extracted steam mass flow rate is constant and uninterrupted during the heat generation period.

Fig. 11 illustrates the daily solar field, packed-bed, and makeup water temperature variation during the operating period – refer to Fig. 2 for the nomenclature and location of each temperature in the system. The temperatures of the makeup water before and after the heat exchanger are represented by T_{mw} and $T_{mw,2}$, respectively. T_5 and T_6 denote the air temperature at the top and bottom of the packed-bed, respectively. The temperatures with the subscript *pb* refer to the packed-bed material. The packed-bed undergoes charging and discharging cycles throughout the days, even on those with low irradiance. In the reference system, the makeup water that follows the heat exchanger can reach temperatures of roughly 150 $^{\circ}C$, as shown in Fig. 11.

At the end of each day, the system ceases to charge the TES due to an insufficient temperature difference in the solar field. However, the packed-bed discharges because the system continues to generate steam, resulting in a decrease in the water level inside the tank. This causes the temperature at the bottom of the packed-bed to decrease. Additionally, the temperature difference between the top and bottom is 83 K on average, which is caused by the thermal inertia of the material.

In comparison with the makeup water temperature $T_{mw,2}$ of the reference system, the temperature one in the improved system decreases according to increasing heat absorbed, as shown in Fig. 11. This is caused by the effect of the implemented control of the makeup water; consequently, the results indicate that $T_{mw,2}$ vary throughout the day. However, during the days with low irradiance $T_{mw,2}$ is within the same range throughout the operating period. Compared to the reference system, the temperature difference between the top and bottom of the packed-bed is higher. Moreover, at the end of each day, the temperature difference between the top and bottom of the energy storage is 87.5 K on average.

The simulation results for day #2, of both the reference system and improved system, were selected to analyse the behaviour of different temperatures in the system.

Fig. 12 shows a detailed view of the temperatures' dynamics, including the TES charging and discharging processes for day #2 of the reference system and the improved system.

As expected, the solar field outlet temperature is the highest in both systems. During the charging cycle, water at the temperature T_2 enters the heat exchanger and transfer heat to the air at T_6. It is important to note that both water and air exit the heat exchanger at similar temperatures. The air flows from the top to the bottom of the TES, so at the bottom of the packed-bed, the copper slag and the air have similar temperatures. The temperature of the copper slag at the top approaches T_5 as the charging process progresses.

Moreover, T_1 results from combining flows at T_3 and T_4, and T_3 is close to the temperature of the kettle reboiler.

During the discharge process, T_6 enters the packed-bed from the bottom at a lower temperature than the copper slag, and the air exits the TES at a similar temperature to the top of the packed-bed. Fig. 12 (a) illustrates that the makeup water, after passing through the heat exchanger, reaches a temperature between 144 $^{\circ}C$ and 157 $^{\circ}C$, resulting in a maximum temperature difference of 137 K. Furthermore, all the heat absorbed by the solar collectors is transferred to the kettle reboiler, causing T_1 to approach the temperature of the tank.

The results indicate that the reference system can generate consistent heat within the heat demand limits. However, a considerable amount of energy is considered waste generation when the peaks exceed the heat demand, and the tank pressure is unstable throughout the operating period.

Fig. 12 (b) provides a detailed view of the temperatures during the same period as the reference system but for the improved system. The temperature $T_{mw,2}$ is approximately 90 $^{\circ}C$, which is lower than that of the reference system. In the reference system, the temperature at the bottom of the packed-bed can reach 160 $^{\circ}C$, whereas in this case, it remains below that value. Compared to the charge and discharge temperature profile of the storage in the reference system, Fig. 12 (b) shows a more linear behaviour in both cases.

4.3. KPIs analysis

The KPIs for the reference and the improved system were calculated based on the description given in section 2.5.1. The KPI results of the reference system calculated across the simulated days are shown in Table 8.

In the same way, the calculation of the KPIs for the improved system are presented in Table 9.

The total energy generated by the reference system throughout the simulation days resulted in 400 *MJ* more than the improved system. However, regarding the energy surplus, the improved system generates only 30 *MJ*, while the reference system generates 518 *MJ*. This means that, although the reference system generates more total energy than the improved system, 518 *MJ* is surplus, i.e., it is not utilised. Moreover, the useful energy in both cases is in the same magnitude range. Furthermore, the results indicate that the improved system presented a total no-cover energy lower than the reference system. A lower no-cover energy means more useful energy is supplied to satisfy the demand. Therefore, the system with the control and operation improvements generates more useful energy, and having a lower air mass flow rate also contributes to a lower fan requirement.

In addition, the KPIs calculated for the SHIP system without the packed-bed TES are shown in Table 10. The results show that throughout the simulated period of five consecutive days, the SHIP system with the TES generates 18.5% more energy than without the TES. Moreover, the system with storage covers 30% more of the demand, and the system generates 20% more energy due to the TES in days with low irradiance.

5. Economic analysis

The SHIP and TES model was used to perform a yearly simulation, applying the heat demand conditions, control, and system parameters listed in Table 7. Additionally, a techno-economic analysis was conducted. Moreover, the yearly analysis was conducted without the TES system to have a comparison.

The assumed price of natural gas was 0.08 $€/kWh$, based on the natural gas price for non-household consumers in Europe reported for the first half of 2023 [41]. In order to determine the required steel wall thickness and calculate the associated steel cost, Eq. (25) was employed. However, upon application of Eq. (25),it was found that s_{steel} was <1 *mm*, due to the unpressurised nature of the vessel, as presented in Table 11. Consequently, a s_{steel} of 3 *mm* was employed, which is a more realistic thickness to comply with the manufacturing process.

Additionally, a boiler efficiency of 0.9 was assumed [39]. An inflation rate of 0.042 [42] and a discount rate of 0.05 [43] were also taken into account. Furthermore, operation and maintenance costs were assumed to be similar to those of parabolic trough collectors, at 5 $€/m^2$ [44]. The calculation was performed for an expected system lifetime of 20 years.

Table 12 presents the results of the annual energy demand and cost of conventional fuel consumption, based on the conditions outlined in Table 7.

Based on the storable energy and the estimated charge/discharge time $t_{ch/dch} = 2200\ s$, the air-to-water heat exchangers require a design thermal power of 90.4 *kW*.

Table 13 compares the energy produced, the gas savings, and the total investment cost of the system with and without the PBTES. Gas savings were calculated using the annual energy generated by the gas price, divided by the boiler efficiency. The results indicate that the system with the TES generates 7% more energy annually and saves 2% more in natural gas consumption. However, the investment is 26% higher when using the TES, primarily due to the air heat exchangers. The payback was calculated for the system with and without the PBTES. The system without the TES has a payback period of 12 years, whereas the system with the PBTES has a payback period of 14 years. It is important to note that the payback period was calculated without considering any economic incentives, which may improve the payback of both systems. Additionally, a calculation was performed to estimate the amount of CO_2 emissions saved by both systems, using a CO_2 emission factor of 0.252 $kg\ CO_2/kWh$ [45].

6. Conclusions

This paper presents a model of an ISG SHIP system coupled with a PBTES model. The TES is integrated to preheat the makeup water of the kettle reboiler using stored energy. The PBTES model uses air as a heat transfer fluid and copper slag as filler material. The system model predicts the dynamics and performance of the complete system, enabling analysis of the influence of incorporating the PBTES.

The size of the solar field and the volume of the TES were chosen based on the results of a parametric study conducted for various cases. A simulation of the system revealed that energy surplus peaks occur when the makeup water pump is activated on days with high irradiance. To address this issue, modifications were made to the system parameters, such as adjusting the air mass flow and makeup water flow. These control improvements enable the system with the packed-bed to generate steady and continuous heat throughout the operating period, even on days with low irradiance. Additionally, the system with PBTES generated 18.5% more energy during the analysed period.

Furthermore, a techno-economic analysis was carried out, which indicated that even though the investment in the SHIP with TES system incurs higher costs than the system without TES, the system enables more energy to be generated annually, resulting in economic benefits in terms of natural gas consumption and savings in CO_2 (emissions)

As future work, different control schemes could be studied to improve the system's behaviour. For instance, the TES air circuit could be used to preheat the pressurised water in the solar field at the beginning of the day.

CRediT authorship contribution statement

Marco A. David-Hernández: Writing – review & editing, Writing – original draft, Visualization, Validation, Software, Methodology, Investigation, Formal analysis, Data curation, Conceptualization. **Ignacio Calderon-Vásquez:** Writing – review & editing, Writing – original draft, Validation, Supervision, Software, Methodology, Data curation, Conceptualization. **Felipe G. Battisti:** Writing – review & editing, Writing – original draft, Supervision, Software, Methodology, Data curation, Conceptualization. **José M. Cardemil:** Writing – review & editing, Supervision, Resources, Project administration, Methodology, Investigation, Conceptualization. **Antonio Cazorla-Marín:** Writing – review & editing, Writing – original draft, Supervision, Resources, Project administration, Methodology, Funding acquisition, Formal analysis, Conceptualization.

Declaration of competing interest

The authors declare that they have no known competing financial interests or personal relationships that could have appeared to influence the work reported in this paper.

Data availability

Data will be made available on request.

Acknowledgements

This work was partially supported by the Research and Development Aid Program (PAID-01-20) of the Universitat Politècnica de València for receiving the Research Fellowship FPI-UPV.2020, as well as the "Programa de Movilidad para estudiantes de doctorado" of the Universitat Politècnica de València. This publication has also been partially supported by the project "DECARBONIZACIÓN DE EDIFICIOS E INDUSTRIAS CON SISTEMAS HÍBRIDOS DE BOMBA DE CALOR", founded by the Spanish "Ministerio de Ciencia e Innovación (MICIN)" with code number PID2020-115665RB-I00, as well as the R&D project SolarSteam4IND (TED2021-130614 A-I00), funded by MICIN/AEI/10.13039/501100011033 and by the European Union NextGeneration EU/PRTR 2021 call. F. G. Battisti acknowledges the funding from ANID/CONICYT through FONDECYT Postdoctorado 2022 #3220792. J. M. Cardemil and F. G. Battisti acknowledge the financial support from project ANID/FONDAP /1523A0006 "Solar Energy Research Center (SERC) Chile".

References

[1] International Energy Agency, "Energy statistics data browser – data tools - IEA." Accessed: Feb 22, 2024. [Online]. Available: https://www.iea.org/data-and-statistics/data-tools/energy-statistics-data-browser?country=WORLD&fuel=Energy consumption&indicator=IndustryBySource.

[2] Farjana SH, Huda N, Parvez Mahmud MA. Industry-specific utilization of solar industrial process heat (SHIP). Nanostructured Materials for Next-Generation Energy Storage and Conversion: Photovoltaic and Solar Energy 2019:409–38. https://doi.org/10.1007/978-3-662-59594-7_14/TABLES/10.

[3] Tasmin N, Farjana SH, Hossain MR, Golder S, Mahmud MAP. Integration of solar process heat in industries: a review. Clean Technologies 2022;4(1):97–131. https://doi.org/10.3390/CLEANTECHNOL4010008.

[4] Bellos E, Arabkoohsar A, Lykas P, Sammoutos C, Kitsopoulou A, Tzivanidis C. Investigation of a solar-driven absorption heat transformer with various collector types for industrial process heating. Appl Therm Eng 2024;244:122665. https://doi.org/10.1016/J.APPLTHERMALENG.2024.122665.

[5] Valenzuela C, Felbol C, Quiñones G, Valenzuela L, Moya SL, Escobar RA. Modeling of a small parabolic trough plant based in direct steam generation for cogeneration in the Chilean industrial sector. Energy Convers Manag 2018;174(June):88–100. https://doi.org/10.1016/j.enconman.2018.08.026.

[6] Frein A, Motta M, Berger M, Zahler C. Solar DSG plant for pharmaceutical industry in Jordan: modelling, monitoring and optimization. Sol Energy 2018. https://doi.org/10.1016/j.solener.2018.07.072.

[7] European Commission. Forthcoming research and industry for Eropean and National Developement of SHIP - FRIENDSHIP. Accessed: Apr 2023;03 [Online]. Available: https://friendship-project.eu/.

[8] European Commission. "Solar heat for industrial process towards food and agro industries commitment in renewables - SHIP2FAIR." Accessed03; 2023 [Online]. Available: http://ship2fair-h2020.eu/.

[9] Barnetche M, González-Portillo LF, Abbas R. Optimum integration of latent heat storage in a solar thermal system for industrial processes: in series or in parallel? Appl Therm Eng 2023;232(June). https://doi.org/10.1016/j.applthermaleng.2023.121090.

[10] Kanojia N, Kaushik S, Singh M, Sah MK. Comprehensive Review on Packed Bed Thermal Energy Storage Systems. Lecture Notes in Mechanical Engineering 2021:165–73. https://doi.org/10.1007/978-981-16-0942-8_15/FIGURES/3.

[11] Seyitini L, Belgasim B, Enweremadu CC. Solid state sensible heat storage technology for industrial applications – A review. J Energy Storage 2023;62:106919. https://doi.org/10.1016/j.est.2023.106919.

[12] Gautam A, Saini RP. A review on sensible heat based packed bed solar thermal energy storage system for low temperature applications. Sol Energy 2020;207(July):937–56. https://doi.org/10.1016/j.solener.2020.07.027.

[13] He X, Qiu J, Wang W, Hou Y, Ayyub M, Shuai Y. A review on numerical simulation, optimization design and applications of packed-bed latent thermal energy storage system with spherical capsules. J Energy Storage 2022;51(March):104555. https://doi.org/10.1016/j.est.2022.104555.

[14] He X, Qiu J, Wang W, Hou Y, Ayyub M, Shuai Y. Optimization design and performance investigation on the cascaded packed-bed thermal energy storage system with spherical capsules. Appl Therm Eng 2023;225(January):120241. https://doi.org/10.1016/j.applthermaleng.2023.120241.

[15] Kumar A, Kim MH. Solar air-heating system with packed-bed energy-storage systems. Renew Sust Energ Rev 2017;72:215–27. https://doi.org/10.1016/j.rser.2017.01.050. no. September 2016.

[16] Kocak B, Paksoy HO. Sensible Thermal Energy Storage in Packed Bed for Industrial Solar Applications. 2019. p. 1–7. https://doi.org/10.18086/eurosun2018.13.06.

[17] Edwards J, Bindra H. An experimental study on storing thermal energy in packed beds with saturated steam as heat transfer fluid. Sol Energy 2017;157(September):456–61. https://doi.org/10.1016/j.solener.2017.08.065.

[18] Zanganeh G, Pedretti A, Haselbacher A, Steinfeld A. Design of packed bed thermal energy storage systems for high-temperature industrial process heat. Appl Energy 2015;137:812–22. https://doi.org/10.1016/j.apenergy.2014.07.110.

[19] Lamrani B, Draoui A. Thermal performance and economic analysis of an indirect solar dryer of wood integrated with packed-bed thermal energy storage system: a case study of solar thermal applications. Dry Technol 2021;39(10):1371–88. https://doi.org/10.1080/07373937.2020.1750025.

[20] Atalay H. Performance analysis of a solar dryer integrated with the packed bed thermal energy storage (TES) system. Energy 2019;172:1037–52. https://doi.org/10.1016/j.energy.2019.02.023.

[21] Cárdenas B, León N. High temperature latent heat thermal energy storage: phase change materials, design considerations and performance enhancement techniques. Renew Sust Energ Rev 2013;27:724–37. https://doi.org/10.1016/j.rser.2013.07.028.

[22] Calderón-Vásquez I, Segovia V, Cardemil JM, Barraza R. Assessing the use of copper slags as thermal energy storage material for packed-bed systems. Energy 2021;227. https://doi.org/10.1016/j.energy.2021.120370.

[23] Mathworks. "MATLAB - El lenguaje del cálculo técnico." Accessed14; 2023 [Online]. Available: https://es.mathworks.com/products/matlab.html.

[24] NIST. "REFPROP." Accessed: Sep. 23 [Online]. Available: https://www.nist.gov/srd/refprop; 2021.

[25] Marco Antonio DH, Antonio CM, José G-M, Jorge PH. Modelling of a solar heat for industrial process (ship) system using fresnel collectors. 2023. p. 396–407. https://doi.org/10.31428/10317/11588.

[26] Frasquet Herraiz M, Silva Pérez MA, Guerra Macho JJ. Tesis Doctoral Ingeniería Energética Recuperación mejorada de petróleo mediante concentración solar. 2021.

[27] T. L. Bergman and F. P. Incropera, Fundamentals of heat and mass transfer, Seventh John Wiley & Sons.

[28] David Hernández MA. Trabajo Fin de Master - Modelado de un sistema de colector solar Fresnel para la generación de vapor de uso industrial. Master Thesis,. Universitat Politècnica de València; 2019.

[29] Cybulski A, Van Dalen MJ, Verkerk JW, Van Den Berg PJ. Gas-particle heat transfer coefficients in packed beds at low Reynolds numbers. Chem Eng Sci 1975;30(9):1015–8. https://doi.org/10.1016/0009-2509(75)87002-3.

[30] Calderón-Vásquez I, Cardemil JM. A comparison of packed-bed flow topologies for high-temperature thermal energy storage under constrained conditions. Appl Therm Eng 2024;238. https://doi.org/10.1016/j.applthermaleng.2023.121934. no. June 2023, p. 121934.

[31] Virtanen P, et al. SciPy 1.0: fundamental algorithms for scientific computing in Python. Nat Methods 2020;17(3):261–72. https://doi.org/10.1038/s41592-019-0686-2.

[32] Van Rossum G, et al. Python 3 reference manual. Nature 2009;585(7825):357–62. Accessed: Jan. 29, 2024. [Online]. Available: https://books.google.com/books/about/Python_3_Reference_Manual.html?hl=es&id=KIybQQAACAAJ.

[33] Solatom CSP. SolatomCSP. Accessed: Jun 2020;08 [Online]. Available: http://www.solatom.com/.

[34] MEPS International. "World steel prices | 3 Year's historical data | MEPS." Accessed26; 2024 [Online]. Available: https://mepsinternational.com/gb/en/products/world-steel-prices?#product-unit-measurement-conversion-form.

[35] Battisti FG, de Araujo Passos LA, da Silva AK. Economic and environmental assessment of a CO2 solar-powered plant with packed-bed thermal energy storage. Appl Energy 2022;314. https://doi.org/10.1016/j.apenergy.2022.118913. no. June 2021, p. 118913.

[36] J. Marti, L. Geissbühler, V. Becattini, A. Haselbacher, and A. Steinfeld, "Constrained multi-objective optimization of thermocline packed-bed thermal-energy storage," Appl Energy, vol. 216, pp. 694–708, Apr. 2018, doi: https://doi.org/10.1016/J.APENERGY.2017.12.072.

[37] Turton R, Bailie RC, Whiting WB, Shaeiwitz JA, Bhattacharyya D. Analysis, Synthesis, and Design of Chemical Processes 2001;40(6):9823. doi: 10.1002/1521-3773(20010316)40:6<9823::AID-ANIE9823>3.3.CO;2-C.

[38] Skills Towering. Cost indices. Accessed: Mar 2024;26 [Online]. Available: https://toweringskills.com/financial-analysis/cost-indices/.

[39] M. Legaz Gómez, "Diseño del almacenamiento térmico en una instalación de 37 kW de la empresa SOLATOM con concentración de energía solar," Master Thesis, Universitat Politècnica de València, 2022. [Online]. Available: https://riunet.upv.es/handle/10251/197184.

[40] Meteotest. Meteonorm. Accessed: Apr 2019;21 [Online]. Available: https://meteonorm.com/.

[41] European Commission. Natural gas price statistics - statistics explained. Accessed: Mar 2024;26 [Online]. Available: https://ec.europa.eu/eurostat/statistics-explained/index.php?title=Natural_gas_price_statistics#Natural_gas_prices_for_non-household_consumers.

[42] European Commission. Eurostat - statistics - annual rate of change. Accessed: Mar 2024;26 [Online]. Available: https://ec.europa.eu/eurostat/databrowser/view/PRC_HICP_MANR_custom_3761882/bookmark/line?lang=en&bookmarkId=4ad27e6f-358a-4a3d-82a0-587d69a833eb.

[43] European Commission. Reference and discount rates. Accessed: Mar 2024;26 [Online]. Available: https://competition-policy.ec.europa.eu/state-aid/legis

lation/reference-discount-rates-and-recovery-interest-rates/reference-and-discount-rates_en.
[44] Baker D, Kamfa I. "Integrating National Research Agendas on Solar Heat for Industrial Processes," no. 731287. 2018. p. 1–38.
[45] Ministerio de Industria Energía y Turismo, "CO2 emission factors and step coefficients to primary energy from different final energy sources consumed in the building sector in Spain (in Spanish)," *Documento Reconocido del Reglamento de Instalaciones Térmicas en los Edificios (RITE)*, pp. 16, 17, 18, 2016, [Online]. Available: http://www.minetad.gob.es/energia/desarrollo/EficienciaEnergetica/RITE/Reconocidos/Reconocidos/Otros documentos/Factores_emision_CO2.pdf.